

POLITECNICO DI TORINO

**Corso di Laurea Magistrale
in Ingegneria Aerospaziale**



Tesi di Laurea Magistrale

Analysis and Optimization of Parking Orbits for a Mars Sample Return Mission

Relatore:

Lorenzo Casalino

Candidato:

Alessandro Novero

Dicembre 2018

To my mother...

Contents

List of Figures	v
List of Tables	vii
1 Mars Sample Return Mission	5
1.1 Introduction	5
1.2 Scientific Objectives	6
1.3 Mars Sample Return Mission Architecture	7
1.3.1 Mars 2020 rover Mission	8
1.3.2 Sample Retrieval Lander	10
1.3.3 Earth Return Orbiter Mission	12
1.4 Landing Site Selection process	14
2 Genetic Algorithms	17
2.1 Introduction to Genetic Algorithm	17
2.2 Genetic Algorithm Terminology	18
2.3 Genetic Algorithm Operating Method	20
2.4 Initial Population	22
2.5 Fitness Function	23
2.6 Selection Process	24
2.7 Reproduction process	25
2.7.1 Crossover	26
2.7.2 Mutation	27
2.8 Stopping Criteria	28
2.9 Genetic Algorithm in MATLAB	30
2.10 Observation about Genetic Algorithm	31

3	Physical Model	33
3.1	Two-Body Motion	33
3.1.1	Conservation of Mechanical Energy	34
3.1.2	Conservation of Angular Momentum	34
3.2	Trajectory Equation and Conic Sections	35
3.2.1	Trajectory equations	35
3.2.2	Conic Section	36
3.3	Patched-Conic Approximation	41
3.3.1	Planetocentric Phase	42
3.3.2	Parking Orbit Capture	42
3.3.3	Parking Orbit Departure	44
3.4	Hohmann Transfer	44
4	Parking Orbit Optimization Problem	49
4.1	Problem Definition	49
4.2	Assumptions	50
4.3	Input & Output Definition	50
4.4	Reference Systems	52
4.5	Calculation Process	54
4.5.1	Stopover Orbit Definition	54
4.5.2	Capture And Escape Conditions Determination	57
4.5.3	Total Velocity Increments Determination	64
4.6	Perturbations Determination	65
4.7	Algorithm Implementation	66
5	Results	69
5.1	Direct Coplanar problem	69
5.1.1	Test problem definition	69
5.1.2	Analytical solution	71
5.1.3	Computational solution	73
5.2	Retrograde Coplanar problem	77
5.3	Right Ascension Variation	81
5.3.1	Identical rotation for capture and escape hyperbolic asymptotes	81
5.3.2	Not identical rotation for capture and escape hyperbolic asymptotes	85
5.4	Non-coplanar problem	88

5.5	Variation of the periapsis distance	91
5.6	Variation of the semimajor axis	94
5.7	Complete problem: implementation of the Descent - Ascent Manoeuvres	97
5.7.1	Variation of the periapsis distance	97
5.7.2	Variation of the semimajor axis	100
6	Conclusions & Future Works	103
	Bibliography	107

List of Figures

1.1	Mars Sample Return Mission phases	9
1.2	Sample Retrieval Lander Design	10
1.3	Sample Fetch Rover Design	11
1.4	Mars Ascent Vehicle Design	12
1.5	Earth Return Orbiter mission phases	13
2.1	Genetic algorithm terminology scheme.	20
2.2	Genetic Algorithm operating method.	21
2.3	Genetic Algorithm influence factors	23
2.4	Roulette selection process	25
2.5	Tournament selection process	25
2.6	One-point crossover operator	27
2.7	Multi-point crossover operator	27
2.8	Uniform crossover operator	27
2.9	Bit-flip mutation operator	28
2.10	Swap mutation operator	28
2.11	Scramble mutation operator	29
2.12	Inverse mutation operator	29
3.1	Relative motion of two bodies	34
3.2	Flight Path Angle and Zenith Angle	35
3.3	Generic conic section geometry	36
3.4	Types of keplerian orbits	37
3.5	Elliptical orbit	39
3.6	Hyperbolic orbit	40
3.7	Capture manoeuvre - Mars SOI	43

3.8	Escape manoeuvre - Mars SOI	43
3.9	Hohmann Transfer	45
4.1	Inertial reference systems - Optimization problem	53
4.2	Noncoplanar stopover orbit launch window geometry	54
4.3	Stopover orbit geometry and flight path angle definition	56
4.4	Geometry for two possible solutions for the capture manoeuvre	60
4.5	Geometry for two possible solutions for the escape manoeuvre	63
4.6	Description of the algorithm implemented via MATLAB	67
5.1	Coplanar problem geometry	71
5.2	Fitness value-Generation plot for the coplanar and symmetrical problem	75
5.3	Direct and coplanar problem: First Solution	75
5.4	Direct and coplanar problem: First Solution - Zoom	76
5.5	Direct and coplanar problem: Second Solution	76
5.6	Direct and coplanar problem: Second Solution - Zoom	77
5.7	Retrograde and coplanar problem: First Solution	79
5.8	Retrograde and coplanar problem: First Solution - Zoom	79
5.9	Retrograde and coplanar problem: Second Solution	80
5.10	Retrograde and coplanar problem: Second Solution - Zoom	80
5.11	Problem geometry for $\alpha_c = 90^\circ - \alpha_e = 0^\circ$	83
5.12	Problem geometry for $\alpha_c = 270^\circ - \alpha_e = 180^\circ$	84
5.13	Problem geometry for $\alpha_c = 135^\circ - \alpha_e = -45^\circ$	86
5.14	Problem geometry for $\alpha_c = 135^\circ - \alpha_e = -45^\circ$ - Zoom	87
5.15	Non-coplanar problem geometry	90
5.16	Non-coplanar problem geometry - Zoom	90
5.17	ΔV for capture and escape manoeuvres - Periapsis Distance	93
5.18	ΔV - Periapsis Distance	93
5.19	ΔV for capture and escape manoeuvres - Semimajor-axis	96
5.20	ΔV - Semimajor axis	96
5.21	ΔV - Periapsis Distance for capture, escape, descent and ascent manoeuvres	99
5.22	ΔV_{TOT} - Periapsis Distance for capture, escape, descent and ascent manoeuvres	99
5.23	ΔV - Semimajor axis for capture, escape, descent and ascent manoeuvres	102
5.24	ΔV_{TOT} - Semimajor axis for capture, escape, descent and ascent manoeuvres	102

List of Tables

3.1	Conic section properties	38
3.2	Planet's SOI with respect to the Sun	41
4.1	Optimization problem input parameters	51
4.2	Optimization problem output parameters and optimized variables	52
5.1	Input data - Direct Coplanar problem	70
5.2	Results of the analytical study.	73
5.3	Results for the direct coplanar problem	74
5.4	Input data - Retrograde Coplanar problem	77
5.5	Results for the retrograde coplanar problem	78
5.6	Input data - Right Ascension variation	81
5.7	Results for $\alpha_c = 90^\circ - \alpha_e = 0^\circ$	82
5.8	Results for $\alpha_c = 270^\circ - \alpha_e = 180^\circ$	84
5.9	Input data - $\alpha_c = 135^\circ - \alpha_e = -45^\circ$	85
5.10	Results - $\alpha_c = 135^\circ - \alpha_e = -45^\circ$	86
5.11	Input data - Non-coplanar problem	88
5.12	Results - Non-coplanar problem	89
5.13	Input data - Variation of the periapsis distance	91
5.14	Results - Variation of the periapsis distance	92
5.15	Input data - Variation of the semimajor axis of the stopover orbit	94
5.16	Results - Variation of the semimajor axis of the stopover orbit	95
5.17	Results - Variation of the periapsis distance of the stopover orbit for capture, escape, descent and ascent manoeuvres	98
5.18	Output data - Variation of the semimajor axis of the stopover orbit for capture, escape, descent and ascent manoeuvres	101

Abstract

One of the most important goals for which the scientific community efforts are focused on is the study of the planets of the Solar System. This is performed in order to evaluate how they formed and evolved during the years. From mid-1960, years of the first mission toward Mars, to nowadays the Red Planet has been a central element for the scientific research. In fact, after the Earth, Mars is the most habitable planet in the Solar System. This can be deduced from several observations concerning the presence of water, the day/night rhythm similar to the Earth one and the presence of an atmosphere that offers protection from cosmic and Sun's radiation. Today, scientists and engineers from all over the world are thinking about a potential future outpost on the Mars surface but particular attention shall be paid on another type of mission. This one, defined as Mars Sample Return, is the highest priority science mission for the next decade as recommended by the 2011 Decadal Survey of Planetary Science [1]. The architecture of this mission is studied in relation to its first goal: take a sample from Martian surface and return to Earth in order to perform detailed studies in well equipped Earth's laboratories. This can permit to answer questions concerning possible human risks and issues related to the Martian environment. The mission technology level and at the same time the total cost is really high involving a complex design for each mission phase. The mission cost is affected by different factors including the trajectory design where this parameter is represented by the propellant consumption. This Master Thesis aims to analyze one of the Mars Sample Return phases, the parking orbit selection within the Martian sphere of influence. The computational capacity of genetic algorithms will be exploited because they can solve optimization problems like the one here presented. The genetic algorithm theory will be introduced after the definition of the Mars Sample Return mission and then, the physical models, exploited for the calculation process, will be described. In the next chapters, the algorithm implemented by MATLAB for the purpose of defining the best parking orbit orientation and the capture/escape injection positions minimizing the propellant consumption will be explained. Subsequently, in order to test and validate the optimization algorithm different study cases will be treated and then the problem relative to the variation of the geometry of the parking orbit will

be discussed. Here, two cases will be treated. The first one will be relative to the periapsis distance variation for a fixed semimajor axis while the second one is referred to the variation of the semimajor axis for a fixed periapsis distance. These two study cases will be then analyzed with the introduction of the descent and ascent phases from the martian surface. Lastly, in order to evaluate the work done and the algorithm accuracy conclusions will be given and future trends will be described.

Introduzione

Uno dei più importanti obiettivi su cui gli sforzi della comunità scientifica sono concentrati è lo studio dei pianeti del sistema solare, al fine di valutare come essi si siano formati e come si siano evoluti durante gli anni. Dalla prima metà degli anni '60, anni delle prime missioni verso Marte, fino ai giorni d'oggi, il pianeta rosso è stato un elemento centrale per la ricerca scientifica. Infatti, dopo la Terra, Marte è definito come il pianeta più abitabile del nostro sistema solare. Questo è confermato da diversi studi riguardanti la presenza di acqua, il ciclo giorno/notte simile a quello della terra e dalla presenza di atmosfera in grado di fornire protezione dai raggi solari e cosmici. Al giorno d'oggi, gli scienziati e gli ingegneri di tutto il mondo hanno l'idea di progettare un futuro outpost sulla superficie marziana ma l'attenzione è principalmente focalizzata verso un altro tipo di missione. Questa, definita come Mars Sample Return, è stata definita dal 2011 Decadal Survey of Planetary Science come la missione con la più elevata priorità scientifica che punta al raccoglimento di un campione di superficie marziana ed al suo successivo ritorno sulla Terra [1]. Qua, il campione verrà studiato in modo dettagliato all'interno di particolari laboratori andando quindi a cercare di dare una risposta alle domande relative a possibili rischi e criticità di una missione umana su Marte e a quelle a cui la comunità scientifica non è ancora riuscita a dare una risposta. Il livello tecnologico della missione, e allo stesso tempo la complessità della stessa, è molto elevato, con un conseguente incremento del costo totale. Questo parametro, uno dei più importanti per la fase di design, è influenzato da diversi fattori tra cui quello preso in riferimento in questa Tesi, ovvero il consumo di propellente definito dalle manovre orbitali che lo spacecraft deve eseguire al fine di raggiungere l'obiettivo di missione.

Lo scopo principale di questo elaborato di Tesi è quello di andare ad analizzare una delle fasi relative ad una missione di Sample Return su Marte, ovvero la fase di selezione dell'orbita di parcheggio all'interno della sfera di influenza marziana. Il primo capitolo di questa tesi sarà dedicato alla definizione della Mars Sample Return Mission andando quindi a contestualizzare il problema di ottimizzazione dell'orbita di parcheggio che verrà poi successivamente trattato. Nel secondo capitolo la teoria degli algoritmi genetici verrà introdotta poichè alla base del metodo di soluzione

del problema sopra citato. Esso infatti ha le giuste caratteristiche per essere risolto da un algoritmo genetico poiché è caratterizzato da un numero elevato di variabili e da uno spazio di ricerca della soluzione molto ampio. Nel terzo i modelli fisici utilizzati durante il processo di calcolo verranno introdotti e successivamente, nel quarto capitolo, sarà definito l'algoritmo di ottimizzazione dell'orbita di parcheggio. Esso, implementato in MATLAB, avrà l'obiettivo, fissate determinate condizioni di cattura e fuga dalla sfera di influenza marziana, di definire l'orientamento dell'orbita di parcheggio e le posizioni delle manovre di cattura e fuga che minimizzano il costo totale di propellente. Il quinto capitolo sarà dedicato all'analisi dei risultati ottenuti. Verranno analizzati diversi casi test per la validazione dell'algoritmo e successivamente, la trattazione relativa alla variazione delle caratteristiche geometriche dell'orbita di parcheggio sarà analizzata. Qui, saranno presi in considerazione due casi, il primo sarà quello relativo alla variazione della distanza del periastro dell'orbita fissato il semiasse maggiore della stessa mente nel secondo, si analizzerà la variazione del semiasse maggiore dell'orbita a fissata distanza del periastro. Successivamente la stessa trattazione verrà analizzata andando a considerare anche le fasi di discesa e ascesa dalla superficie marziana. Infine, nell'ultimo capitolo le conclusioni e gli sviluppi futuri verranno esposti.

Chapter 1

Mars Sample Return Mission

1.1 Introduction

Mars has been one of the most fascinating planets for humanity since the time of the ancients. From 1964, when the Mariner 4 fly-by returned 21 images of the red planet, to nowadays, there have been several dozen spacecraft sent to Mars, of which 15 have been successful. Each mission performed has enabled improvements concerning the scientific and technical knowledge about the Red Planet. Many studies were performed but, as is typical of the progress of science, these investigations have raised more questions than they have answered. Thus, Mars remains a high-priority target for ongoing exploration. Many people are wondering why Mars is at the center of the study of the scientific community. The answer can be explained through these primary reasons:

- Mars is the most Earth-like planet in the Solar System
- Mars is the most accessible planet in the Solar system
- Mars is a potential target for an eventual and future human exploration

The last reason is referred to the possible next step for humanity, but before, scientists and engineers must improve their knowledge about the Martian environment defining all the possible risks and issues for human health. Past missions, like Mars Exploration Rover, have made exceptional discovers about the presence of water, Carbon composites trace into Mars rocks and the measure of fluctuations of methane level into Mars atmosphere during the seasons. These discoveries have made by means of different types of mission characterized by four systems: fly-by probes, orbiters, lander and rover [5]. Fly-bys were the very first missions. Their goal was to simply

flew by Mars and taking as many pictures as possible on their way past. Orbiters have allowed to analyze Mars atmosphere at different heights while landers and rovers have studied the Mars atmosphere on a different perspective. They have studied not only the lower atmosphere layers but also the Mars soil. Nowadays, scientific progress has led to the formulation of new mission concepts where airplanes, balloons, surface explorers and sample return vehicles can be used. In this section, the attention is focused on the last concept, where the first aim is to return samples from Mars to Earth. This mission, called Mars Sample Return, can generally be designed in three different architectures based on the type of Mars sample that must be collected. These are:

- Fly-by
- Touch-and-go
- Surface collection

In Fly-by missions, planet samples are collected without touching its surface thus, the primary goal is to collect dust from planet atmosphere. The spacecraft flies on a low orbit a single or more times where the samples are collected and then return to Earth. The technology level needed for this mission is lower because the spacecraft does not touch the planet surface and then no landing technologies are required. In a touch-and-go mission, the spacecraft briefly lands on the planet surface, collects the sample and moves into another collection site or return to the Earth. The cost of this mission is higher than flyby one because landing technologies are required. Lastly, surface collection mission is the most complex. It is composed of different phases performed by different systems. The systems involved are a rover, that collects the sample, and a lander. This last system contains an ascent vehicle that permits to send the sample into the Mars orbit and then, after a rendezvous manoeuvre with an orbiter, the samples will return to Earth. Sample return vehicles are heavier respect the ones in flyby and touch-and-go missions. Moreover, they can be designed in different ways depending on science goals, budget, desired complexity, reliability and other parameters. This chapter is focused on this concept in reference to the Mars Sample Return mission that NASA and ESA are designing.

1.2 Scientific Objectives

As written before, the idea of the Mars Sample Return Mission was proposed in order to search answers relative to the questions raised from past missions investigations. Thus, this mission must be designed in order to achieve different scientific goals related to questions that keep the focus on the Red Planet. The selection process for the MSR primary goals choice has lasted

for two decades in which many previously international priorities have been defined. Nowadays, the attention is focused on seven objectives defined by the International MSR Objectives and Samples Team (iMOST) [2]. This team must evaluate and update the sample-related science and engineering objectives of the Mars Sample Return campaign. Moreover, The iMOST team must define the types of measurements and the types of samples that can best address the objectives. The seven objectives, cited before, are:

1. Interpret the primary geologic processes and history that formed the martian geologic record, with an emphasis on the role of water
2. Assess and interpret the potential biological history of Mars, including assaying returned samples for the evidence of life.
3. Quantitatively determine the evolutionary timeline of Mars.
4. Constrain the inventory of martian volatiles as a function of geologic time and determine the ways in which these volatiles have interacted with Mars as a geologic system
5. Reconstruct the processes that have affected the origin and modification of the interior, including the crust, mantle, core and the evolution of the martian dynamo
6. Understand and quantify the potential martian environmental hazards to future human exploration and the terrestrial biosphere.
7. Evaluate the type and distribution of in-situ resources to support potential future Mars exploration

These seven objectives provide a framework for demonstrating how the first set of returned martian samples would impact future martian science and exploration. They also have implications for how analogous investigations might be conducted for samples returned by future missions from other solar system bodies, especially those that may harbor biologically relevant or sensitive material. The list above is constantly updating due to the scientific community priorities. Moreover, Mars environment varies on the basis of the location taken into account so the landing site selection has a key role. The landing site selection for NASA-ESA Mars Sample Return Mission will be described in the next sections.

1.3 Mars Sample Return Mission Architecture

As described before there are three different ways to perform a Mars Sample Return mission but, for the scientific objectives listed in the above section, only the third one can be considered. In

the past, many studies have been done and different architecture and concept have been designed [8][9][14]. During the years, the idea of a Mars Sample Return has been taking shape and on April 26 2018, NASA and ESA signed a Statement of Intent to work together to formulate, by the end of 2019, a joint plan for the retrieval mission. Thus, nowadays, the Mars Sample Return is a joint collaborative project between two of the most important space agencies from all over the world. This decision is linked to the scientific goals and the idea of a future human outpost on the Red Planet which remains the primary goal for the next future. The proposed mission architecture [4] can be defined as a campaign where a sequence of specific missions will permit to take the martian Sample and then return to Earth. Thus, the entire mission can be divided into three different submissions. These are:

- Mars 2020 Rover Mission
- Sample Retrieval Lander
- Earth Return Orbiter

The Mars 2020 Rover mission, led by NASA, is the first element of Mars Sample Return campaign which is planned for July 2020 and it aims to catch samples of Martian rocks during its nominal 1.25 Mars-year mission. After the sample collection phase, it will cache them in a defined depot. The second mission is characterized by the Sample Retrieval Lander system that will contain the Mars Ascent Vehicle (MAV) and the Sample Fetch Rover (SFR). The second element will collect the sample from its depot and then it will return them to MAV where they will be stored in the Orbital Sample (OS) element. This one will be the MAV payload launched by this ascent vehicle into a nominally circular orbit. At this point, the third missions will start. It will composed by the ERO element that will be able to rendezvous with the Mars Ascent Vehicle, collect the Orbiting Sample and come back to Earth where the OS will be studied in a well-equipped laboratory. This facility is called Mars Returned Sample Handling (MRSH) and it is composed of all post-landing handling, the sample receiving and curation activities. Here, scientists will analyze the Mars sample and will try to expand the knowledge about the Red Planet answering questions that have no answer. The sequence of the different mission phases can be observed in Fig.1.1.

1.3.1 Mars 2020 rover Mission

The Mars 2020 rover mission is led by NASA inside the Mars Exploration Program (MEP). It aims to a long-term effort of robotic exploration of the Red Planet [32]. This mission is timed for its first launch opportunity in July/August 2020. In these months Earth and Mars will be in a good

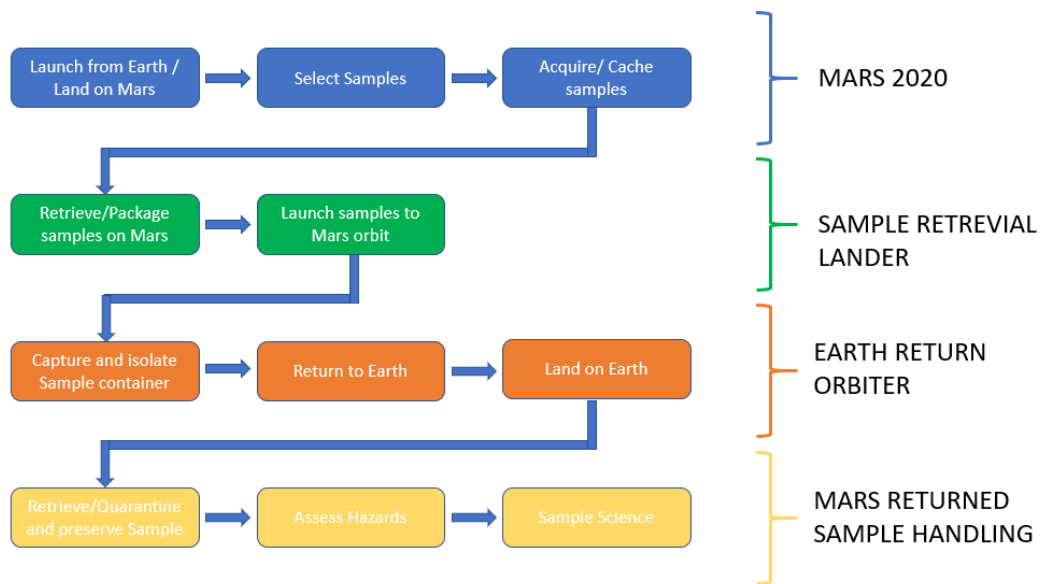


Figure 1.1: Mars Sample Return Mission phases

position relative to each other for landing on Mars. This mission is designed in order to achieve four scientific goals:

- Determine whether life ever arose on Mars
- Characterize the climate of Mars
- Characterize the geology of Mars
- Prepare of human exploration

Moreover, through a new type of systems as the drill, Mars 2020 Rover will be able to collect samples of the most promising rocks on the Mars surface that with the support of other future missions will permit to bring them to Earth. This mission will also provide the opportunity to gather knowledge and demonstrate new technologies that address the challenges of future expeditions to Mars. For example, an oxygen production system from the Martian atmosphere will be tested. The atmosphere on Mars is composed of 96 per cent carbon dioxide so this technology demonstration will help mission planners to test ways of using Mars’ natural resources to support human explorers and improve designs for life support, transportation, and other important systems for living and working on Mars. At the same time, in order to keep mission costs and risks as low as possible EDL and surface operations technology exploited for Curiosity Rover will be reused.

1.3.2 Sample Retrieval Lander

The Sample Retrieval Lander or Sample Return Lander is the second mission that will be launch to accomplish the goals of the Mars Sample Return Mission. It is under design by ESA and NASA (In Fig.1.2 is represented a possible design) and it is principally composed by:

- Sample Fetch Rover
- Mars Ascent Vehicle

These elements have a key role inside the entire Sample Return Mission because the first one must catch the sample left behind by Mars 2020 rover while the second one permits to bring the samples into a specific orbit around Mars.

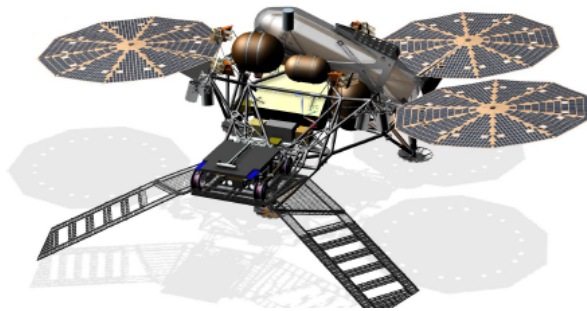


Figure 1.2: Sample Retrieval Lander Design

Sample Fetch Rover

The Sample Fetch Rover is one of the key elements of the Mars Sample Return campaign [10]. When the Sample Retrieval Lander will land on Mars surface, the Sample Fetch Rover will go down from the platform in order to perform two activities:

- To collect the sample tubes left by NASA's Mars 2020 Rover
- To bring the sample tubes to the Sample Retrieval Lander where a dedicated robotic arm will move them to the Mars Ascent Vehicle.

Moreover the Sample Fetch Rover must be characterized by the following properties:

- Lightweight
- high mobility capabilities

- high reliability

The first property is important in order to not exceed the mass limitations of entry descending and landing system. Thus, its maximum mass is fixed and is equal to $120kg$. At the same time, the Rover must not have a big volume because it must be stowed inside the SRL that for this system have a maximum volume of $1m^3$. The high mobility capabilities are important during the navigation phases, where the Sample Fetch Rover will transverse from its landing site to the location of a sample cache left behind by the previous rover mission. This rover will be designed for an average traverse distance of $150 - 250m/sol$ for a maximum mission duration of $210sol$. Moreover, SFR will be autonomous during the navigation phases where the process of image processing will support the autonomous driving. Lastly, the high reliability will allow to SFR to survive into the Martian environment whose is characterized by vary criticalities as dust storms. A possible design of the Sample Fetch Rover is shown in Fig1.3.

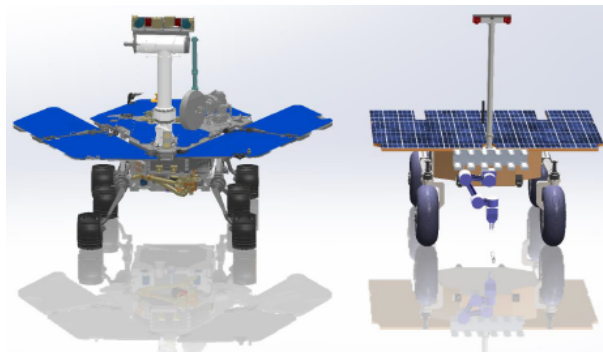


Figure 1.3: Sample Fetch Rover Design

Mars Ascent Vehicle

The Mars Ascent Vehicle or MAV is one of the largest technology development risks for the Mars Sample Return mission. It must be developed in order to survive a variety of conditions including the interplanetary flight, entry descending and landing phases. Moreover, it must survive in the Mars surface environment while maintaining the ability to deliver its payload, the Mars sample, into a low Mars orbit. At the same time, as written before relative to the Sample Fetch Rover, it must be light. This permits to not exceed the mass limitations of entry descending and landing system. Many studies about Mars Ascent Vehicle design were executed during the years [9][14]. Now, NASA and ESA engineers are studying a MAV design characterized by a single-stage with

hybrid propulsion. This type of design should allow the design of a Mars Ascent vehicle characterized by a gross liftoff mass of 300 – 400kg.

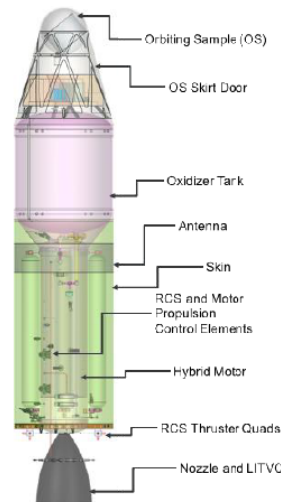


Figure 1.4: Mars Ascent Vehicle Design

Another important element of the Sample Retrieval mission is the Orbiting Sample (OS) container. It will be contained inside the MAV and it can be defined as the element in which The Sample Fetch Rover will move the Mars tubes containing the Mars samples. Thus, during the rendezvous manoeuvre the OS will move from the MAV to the Earth Return Orbiter and then it will return to Earth. In each phase, the OS must be able to maintain samples within environmental constraints.

1.3.3 Earth Return Orbiter Mission

The Earth Return Orbiter or ERO is the key element of the third phase of the mission [12][13]. This mission will set three new records:

- First return from another planet
- First rendezvous around Mars
- First bio-contained sample return

The spacecraft, entering inside the Mars sphere of influence, will move from its hyperbolic trajectory to a specific circular or elliptical parking orbit. At this point, it will rendezvous with the Mars Ascent Vehicle in order to move the Orbiting Sample from the MAV to the ERO and then it

will return to Earth. The transfer of the Orbiting sample is one of the most complex phases of the entire mission. Here, the samples will be sealed into a bio-container which permits their insulation and thus, their properties will be maintained to their original conditions. Once the spacecraft will reach the Earth, the Entry Vehicle (EEV) will be released on an Earth-impacting trajectory in order to land at a designated site where the sample will be taken and transferred to a Sample Receiving Facility for storage, opening and evaluation. At the same time, the rest of the spacecraft will perform an Earth avoidance manoeuvre in order to not impact on the Earth surface. Furthermore, Earth Return Orbiter must be designed in order to be able to perform telecommunications operations between systems on Mars surface and ground stations on Earth. Telecommunication operations must be performed during each mission phase so the parking orbit selection must taken into account these operations. Studies have shown that in order to support telecommunications relay and rendezvous operations the orbiter would be inserted into a highly elliptical orbit and then aerobrake down to potentially a 500 km circular orbit. The phases of the ERO mission are shown in Fig.1.5.

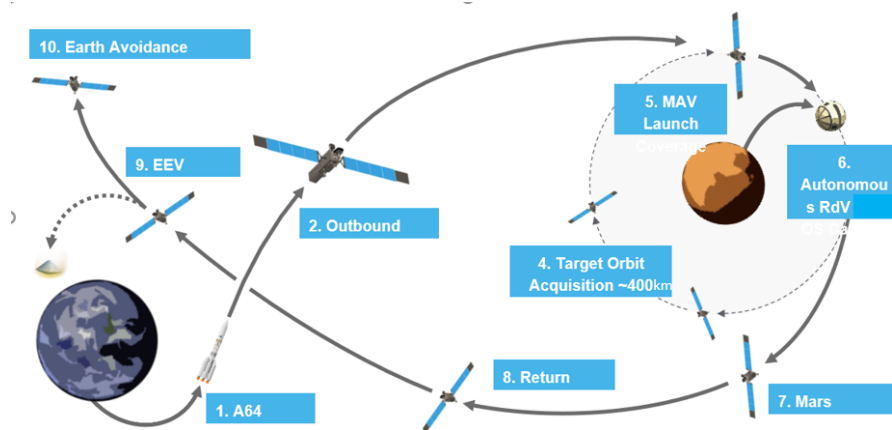


Figure 1.5: Earth Return Orbiter mission phases

The concept of this orbiter is under study by ESA engineers. Many designs have been studied with chemical, hybrid and electric propulsion systems with particular attention to the system mass. In fact, as written before for the MAV and for the SFR, the system mass is a critical driver for the feasibility of Mars return. Lastly, the Earth Entry Vehicle is another important element of the Mars Sample Return mission. This system will permit the return to Earth of the sample tubes and so it must survive during the entry, descending and landing phases on Earth atmosphere. Many studies are performing about the EEV where, the first goal is to design a system able to land on the Earth surface without compromising the samples properties.

1.4 Landing Site Selection process

The Landing site selection process is one of the most important phases of the mission design. This choice must be analyzed through a trade-off study where risks, costs and scientific objectives must be considered. The landing site selection process for the Mars Sample Return Mission, defined by ESA and NASA, is referred to the Mars 2020 Rover mission which is the first one to be performed [3]. The choice of the best landing site is principally affected by two types of constraints:

- Engineering constraints
- Scientific constraints

The first ones limited the location on Mars where the rover can be delivered in terms of latitude, longitude, elevation, radar reflectivity, thermal inertias and albedo while the second ones are referred to the scientific objectives and their priorities. The selection process started from about 30 candidates and after a series of three workshops, where the entire scientific community was involved, the number of suitable landing sites has now narrowed to three. These are:

- Jezero Crater
- Columbia Hills
- NE Syrtis

The three remaining landing site candidates for the Mars 2020 rover mission represent diverse geological settings that all offer the potential for preservation of biosignatures that can confirm the presence of life on Mars in its history. Thus, the Martian samples that would be returned from any of the final landing site candidates would represent an abundance of opportunities for scientists for decades.

Jezero Crater

Jezero Crater is interpreted to represent a delta formed in a crater lake. It is situated $18.4386^{\circ}N$ and $77.5031^{\circ}E$ at an elevation of $-2.64km$. This landing site could be chosen for its probability to find traces of organic material which would be valuable in the search of ancient biosignatures. This high probability is given by the delta that could contain materials from a diverse set of environments.

Columbia Hills

The Columbia Hills is the only landing site previously visited by a past mission, in fact, it was the Spirit rover landing site in 2004. The landing location is centred at $14.5478^{\circ}N$, 175.6255° at an elevation of $-1.93km$. Past studies performed by Spirit Rover showed that this site is characterized by the presence of silica deposits that could contain evidence of microfossils and/or microbially produced by organic matter.

NE Syrtis

The NE Syrtis site is situated at $17.8899^{\circ}N$ latitude and $77.1599^{\circ}E$ longitude at $-2.04km$ elevation. This landing site represents a deep crustal setting in which water reacted with rocks, possibly providing a hydrothermal setting analogous to inhabited environments on Earth. This type of terrain could contain evidence for igneous, hydrothermal and sedimentary environments.

Chapter 2

Genetic Algorithms

2.1 Introduction to Genetic Algorithm

Many common applications of predictive analytics, from customer segmentation to space mission design, arise from complex relationships between features. The selection of these features, also called variables, is the process of finding the most relevant one for a predictive model. Genetic algorithms are heuristic search methods inspired by Darwin's Evolution Theory that through the use of natural selection, adaptation and survival laws find the best solution to optimization problems. Since the mid-1990s scientists and researchers have studied artificial intelligence and evolutionary computation, trying to implement computer programs that could simulate natural world processes. The first genetic algorithm software was created by Nils Barricelli in 1954 with the goal to create and develop artificial life and not to solve optimization problems or simulate biological evolution. Barricelli's work was followed by other scientists as Alexander Fraser who, in 1957, was the first to have the idea of creating a computer model of evolution. The genetic algorithm version that is known today was for the first time written in the 1960s by John Holland, a professor at the University of Michigan. Holland's version, described in his famous book *Adaptation in natural and Artificial System*, involved a simulation of Darwin's principle relative to the survival of the fittest, as well as processes of crossover, recombination, mutation and inversion that are the basis of genetics. Research on genetic algorithms rapidly increased in the 1970s and 1980s due to advances in technology. Scientists involved in these types of study began to realize the limitations of conventional programming and optimization methods for solving complex problems and thus they found that genetic algorithms were a way to find solutions to these problems. Conventional optimization methods cited before are three:

- Calculus-based

- Exhaustive search
- Random search

Calculus-based methods can be divided into two categories: direct and indirect. The first one follows the direction of the gradient towards a local maximum or minimum value while the second one takes the gradient of the objective function, sets it equal to zero, then solves the set of equations that result. These methods are good for local optimal search and can be useful when derivatives of the objective functions existed. Exhaustive search methods test every single value belonging to a defined finite search space in order to find the maximum or minimum value of the objective function. It is the least efficient of all optimization algorithms due to the high calculation time when a complex problem is considered. Lastly, random search algorithms are based on the random choice of some representative samplings from the search space. These samplings are then analyzed and the optimal value is chosen. Using this type of algorithms the solution cannot be the optimal one of the entire search space. As written before, natural evolution mechanisms can be used to solve some of the most difficult computational problems that concern solution definition within a huge number of possible alternatives. Indeed, biological evolution process can be treated as a research method where the desired solutions are adapted organisms with strong survival and reproduction capabilities in changing environments that pass to next generations their genetic properties. In this contest, each organism can be considered as a solution because it survives in its environment through the development of behaviours and skills that are even the evolution result. Genetic algorithms are based on Darwin's studies described in his book *On the origin of species by means of natural selection* wrote in 1859. Thus, this type of algorithms is based on Darwin's Theory of evolution, where elements with strong adaptive skills have much chances to survive in a changing environment and have many probabilities to transmit their properties to their future generations. Through this principles, genetic algorithms are able to perform a heuristic solution research into zones where there are more probabilities to find better solutions but at the same time don't neglect worst ones where a small number of resources are used. Nowadays, genetic algorithms are used in different research fields where optimization problems must be resolved.

2.2 Genetic Algorithm Terminology

Since genetic algorithms are designed to simulate a biological process, much of the relevant terminology is borrowed from biology and genetics. Basic terminology is composed of:

- *Population*: it is a subset of all the possible solutions to the given problem.

- *Individual or chromosome*: it refers to a numerical value or values that represent a candidate solution of the optimization problem. to the problem that the genetic algorithm is trying to solve
- *Gene*: it is one of the elements of an individual.
- *Feature or allele* : it is the value a gene takes for a particular chromosome
- *Genetic operator*: it is a process aims to modify the genetic composition of the offspring.
- *Fitness function*:it is defined as a function which takes the solution as input and produces the suitability of the solution as output.
- *Son*: it is the results of the reproduction process that belongs to the next population as a member.
- *Genotype*: it is the population in the computation space.
- *Phenotype*: it is the population in the actual real world solution space. For simple problems Phenotype coincides to Genotype.
- *Decoding - Encoding*: Decoding is a process of transforming a solution from the genotype to the phenotype space, while encoding is a process of transforming from the phenotype to genotype space.

Many terms of the list above will be used in the next sections in order to properly describe every single process of a genetic algorithm. A schematic overview of this terminology is shown in Fig. 2.1 where the difference between some terms can be easily noted.

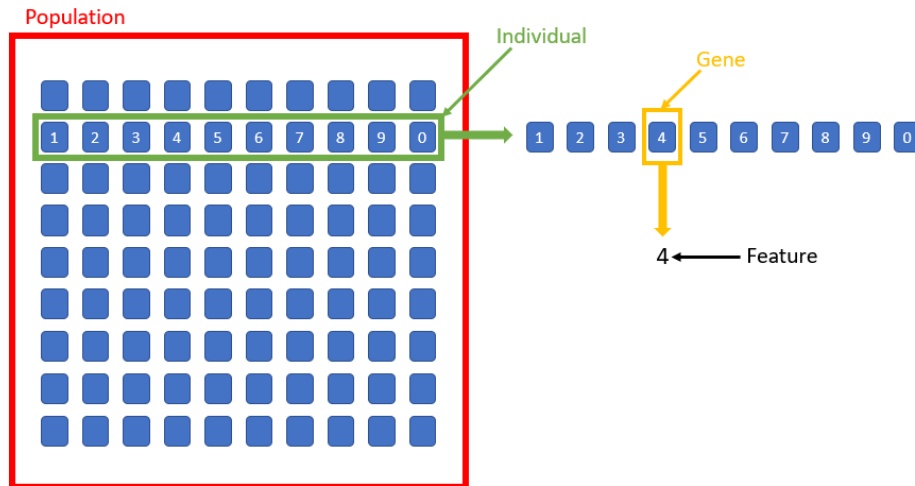


Figure 2.1: Genetic algorithm terminology scheme.

2.3 Genetic Algorithm Operating Method

As written before genetic algorithms are based on natural selection laws, where individuals reproduction mixes their genetic heritages in order to generate new individuals that have got genetic properties derivated by parents ones. The natural selection process permits to survive only to stronger and more adaptive fellows so that the species evolves over time, generation after generation. Genetic algorithm operating principle, as represented in Figure 2.2, can be described by the sequence of different phases. The most important are :

1. **Creation of the initial population.** This first phase is the generation of first individuals where this process can be random or defined by the user with different options.
2. **Fitness Value definition.** In this phase, a score, called raw fitness score, is assigned to each individual on the basis of its properties.
3. **Raw fitness score scaling.** This phase permits to convert them into a more usable range of values. These scaled values are called expectation values.
4. **Parents selection.** Best members, called parents, are chosen on the basis of their expectations.
5. **Elite members selection.** They have lower fitness value and thus they are directly passed to the next generation.

6. **New generations creation.** These are composed of children where every child is produced either by making mutation (random changes to a single parent) or crossover (combining pairs of parents).

7. **New population generation.**

The iter above described is multistep, thus it stopped when a stopping criterion is met. Each phase has a key role inside the determination of the optimal solution process. In order to find the best solution in the most efficient way , the user can be customized options and parameters that affect the choice of parents and the creation of new generations.

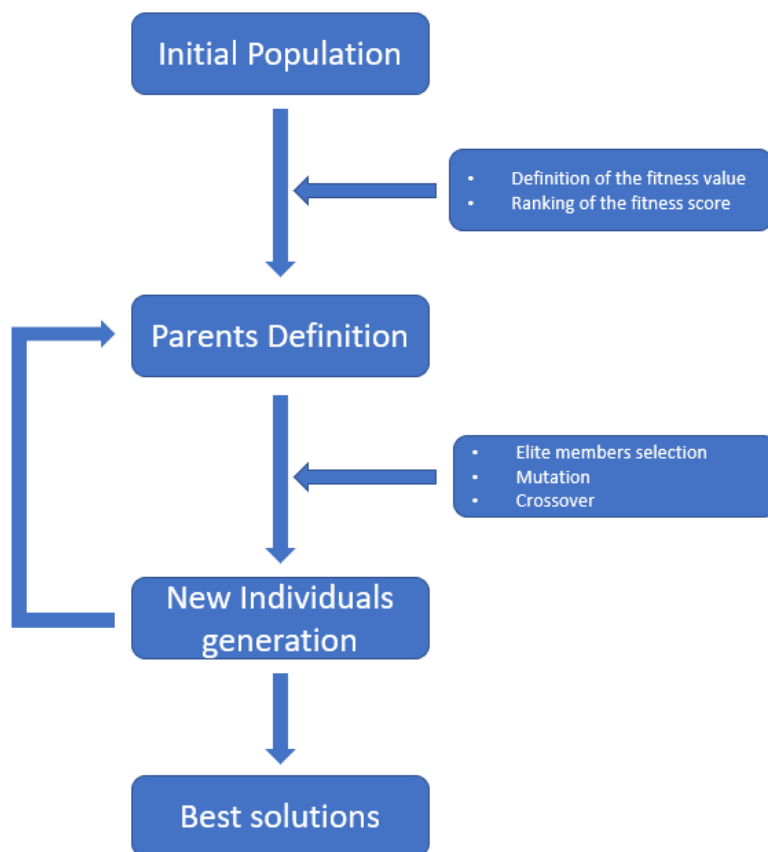


Figure 2.2: Genetic Algorithm operating method.

2.4 Initial Population

The first step in the functioning of a genetic algorithm is the generation of the initial population. It is composed by an initial set of individuals that can be randomly defined or properly set within a specific range by the user. This first phase has a key role inside the algorithm because it affects the efficiency of the optimal solution definition process. Each member of this population encodes a possible optimal solution and then, it is important to consider two key parameters:

- population size
- members type

These ones are related and are two of the most important topics to consider when an evolutionary or a genetic algorithm is used. Researchers usually argue that a small population size could guide the algorithm to poor solutions and that a large population size could make the algorithm expend more computation time in finding a solution. This is not always true because the initial population is not only factor that influences the algorithm performance. In fact, there are other parameters that can affect the efficiency of genetic algorithms [17]. These are:

- Search space
- Fitness function
- Diversity
- Problem difficulty
- Selection pressure
- Number of individuals

Past studies have demonstrated that the right number of individuals may increase the probabilities to find a "good" solution. In the opposite case, the convergence of the algorithm is not assured and then the solution cannot be the optimal one. Moreover, when some information concerning a possible solution is known, it can be a good method to insert them into the initial population and thus narrow the search space. Members diversity is another important parameter to consider when a genetic algorithm is used and it can be referred to the average distance between individuals in a population. It must be taken into account when no information about the possible optimal solution is known. In this case, it has an important role because a greater diversity may lead to greater possibilities to find solutions. Selection pressure is related to members diversity and it can

cause a premature convergence. This occurs when selection pressure is characterized by a high value. Lastly, it can be demonstrated that problem difficulty can affect the algorithm efficiency. If the problem is complex then may be necessary to have a bigger initial population. In the opposite case, a smaller number of initial individuals may be sufficient to find the optimal solution.

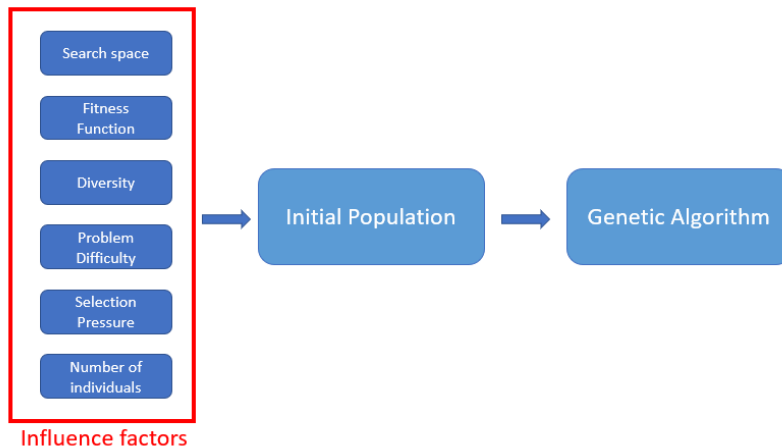


Figure 2.3: Genetic Algorithm influence factors

2.5 Fitness Function

As written before, the fitness function is one of the factors that influence the initial population properties and then it may affect the algorithm converge or divergence. It is defined as a function which takes a problem candidate solution as input and generates as output a value representing how good is the input solution respect to the problem. The fitness function must be properly defined because it is the function that is evaluated at each step for every population member. In fact, a "good" fitness function can have a positive effect on the algorithm computational speed. On the basis of the problem complexity, it can be possible to choose a fitness function equal to the objective one where the last one is the one that must be minimized from the genetic algorithm. This can be done when the following conditions are verified:

- Small number of variables
- Small number of constraints
- Low complexity

Lastly, it is important to define how to properly write the fitness function. Surely, it must have the following characteristics:

- It should be clearly defined and efficiently implemented
- It should be sufficiently fast to compute.
- It must measure how fit and how good is a given solution. At the same time, it must measure how fit individuals can be produced from this given solution.
- It should generate intuitive results

2.6 Selection Process

When fitness assignment process is performed every individual is evaluated by means of the fitness function. After that, another key process must be executed. This one, called *Selection process*, aims to choose, through a specific selection operator, the best individuals. This is the first step of the new population generation based on the reproduction process. The individuals choice is based on their fitness score, where it represents the individual capacity to survive into the problem environment. Thus, in accord with natural laws, they can be defined as stronger individuals. A key element inside the selection process is the selection function. It must be defined on the basis of the given problem and its choice can be executed between the following functions:

- Stochastic Uniform
- Uniform
- Roulette
- Tournament
- Reminder

The stochastic Uniform selection method is the default one and it lays out a line in which each parent corresponds to a section of the line of length proportional to its scaled score. When this method is used the algorithm moves along this line in steps of equal size and during each step a parent from the section is allocated. The Roulette selection function is based on the roulette wheel game. The whole wheel is divided into different sections in which each one corresponds to an individual and the size of the section is proportional to its expectation. This method is shown in Fig.2.4. The tournament selection method generates parents through a process where a group of two or more individuals are confronted and the best one becomes a parent. In this case, it is possible to decide tournament size and so how many individuals are confronted at the same time.

This process is the one used in this Master thesis and it is represented in Fig. 2.5. The remainder selection method is another deterministic option. It performs two-step, the first one is the selection of the parents by means of the integer part of the scaled value while the second one is the selection of additional parents using the fractional parts of the scaled score. This process is the same that is executed in the stochastic uniform selection. Lastly, the uniform selection process is the one used for debugging and problem testing. It is based on expectations and the number of parents that must be reached. After this process, other individuals are chosen as Elite ones through an elitism selection. These individuals are directly passed into the next generation as parents. The number of Elite individuals can be chosen from the user and it affects the algorithm behaviour.

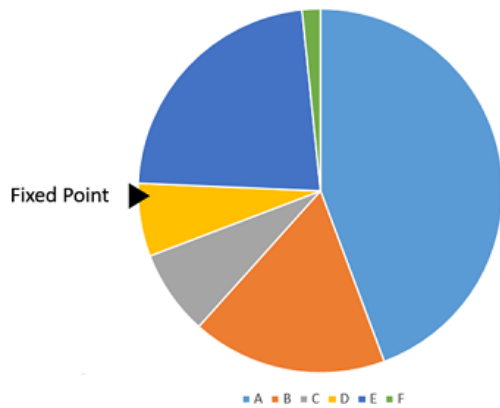


Figure 2.4: Roulette selection process

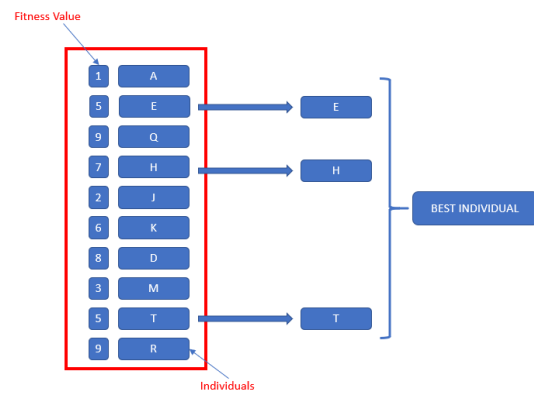


Figure 2.5: Tournament selection process

2.7 Reproduction process

The reproduction process can be defined as the set of operations which permit to generate a new population from a previous one. After the selection process, by means of parents are chosen, individual's properties are recombined in order to create sons which have better genes compared to their parents. From this new generation, a second new generation is produced by the same process and so on. Thus, this process permits to generate better individuals and so better solutions. This process of recombination exploits two types of reproduction techniques that will be treated in the next two sections:

- Crossover
- Mutation

2.7.1 Crossover

Crossover is a reproduction technique where once two individuals are randomly selected, their properties are recombined to get new individuals belonging to the new generation. The number of sons generated from this process can be chosen by the user and the default value is 4. Moreover, the percentage of the entire population that is made up of crossover children can be chosen too. This option is called crossover fraction and it is represented by a number between 0 and 1. A value of 1 means that all children are crossover ones, while a crossover fraction of 0 means that all children are mutation ones. Since the number of individuals of the next generation cannot exceed the number of individuals in the previous one when the size of the current population is the same as the old one the process is stopped. There are different crossover operators, the most important are:

- One-point Crossover
- Multi-point Crossover
- Uniform Crossover

One-point crossover, represented in Figure 2.6, is the operator where a random crossover point is selected and the tails of its two parents are swapped to get new off-springs. This crossover point is the same for both parents. The second technique, the multipoint crossover, represented in Figure 2.7, is a generalization of the one-point crossover wherein alternating segments are swapped to get new off-springs. This can be thought of as the evolution of the technique explained above. Lastly, in a uniform crossover, represented in Figure 2.8, the chromosomes are not divided into segments but essentially a coin is flipped for each chromosome in order to decide whether or not it will be included in the offspring. Traditionally, genetic algorithms have relied upon 1 and 2-point crossover operators. Moreover, it can be demonstrated that a large number of crossover point can improve the efficiency of the algorithm. Nowadays, new studies are introducing new types of genetic algorithms, called adaptive ones, where they decide which is the optimal crossover technique to use.

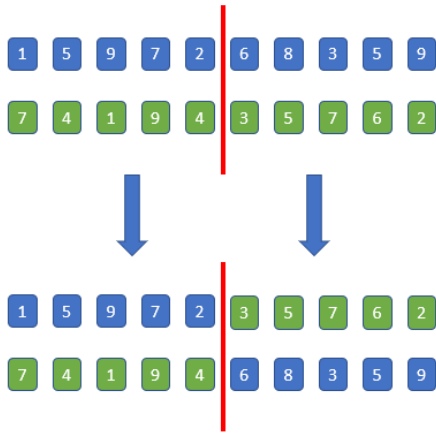


Figure 2.6: One-point crossover operator

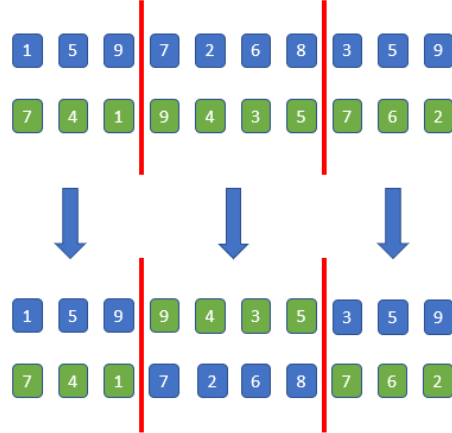


Figure 2.7: Multi-point crossover operator

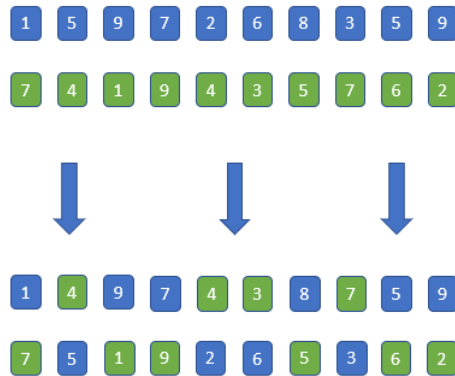


Figure 2.8: Uniform crossover operator

2.7.2 Mutation

Mutation is a genetic operator analogous to a biological one that has the characteristic to maintain genetic diversity generation after generation. During this process, each parent is randomly altered from its initial state in order to generate new offsprings. In this way, low diversity is avoided and then the search space is wide. In general, mutation process can be thought as a process where in order to decide if a feature will be mutated, a random number with a value between 0 and 1 is generated. If this one is lower than a value called mutation rate the variable is flipped. The mutation rate by default is defined as the inverse number of individual’s features but this value

can be set by the user too. Using default value statistically at least one feature of each individual is changed. There are different mutation operators, the most important ones are:

- Bit flip mutation
- Swap mutation
- Scramble mutation
- Inversion mutation

Bitflip mutation, represented in Figure 2.9, exploits the operating method written above where a feature is mutated if its value is lower than the mutation rate. This operator is often used when a binary encoded genetic algorithm is implemented. The second mutation operator, the Swap mutation, is based on the interchange of the value of two different features. This operating process is shown in Figure 2.10. Scramble mutation operator, represented in Figure 2.11, is based on the following operating method: from an entire chromosome, a subset of genes is chosen and their values are scrambled or randomly shuffled. Lastly, in Inversion mutation, as shown in Figure 2.12, a subset of genes is selected like in scramble mutation, but instead of shuffling the subset, the entire string in the subset is inverted.

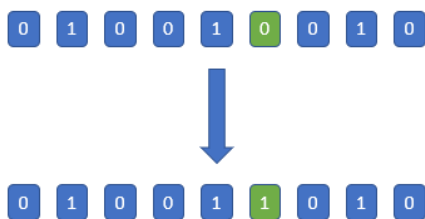


Figure 2.9: Bit-flip mutation operator

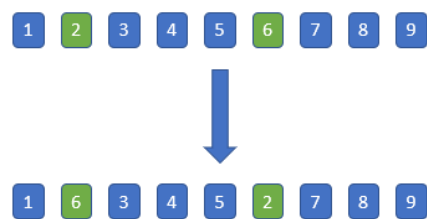


Figure 2.10: Swap mutation operator

2.8 Stopping Criteria

Unlike derivative search methods that terminate when a local optimum is reached, Genetic algorithms are stochastic search methods that could in principle run for ever. In practice, a termination criterion is needed. Stopping criteria determine what causes the algorithm to terminate and so which are the conditions that stopped the algorithm. Many types of stopping criteria may be

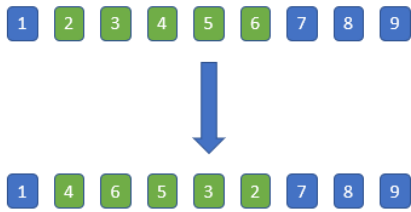


Figure 2.11: Scramble mutation operator

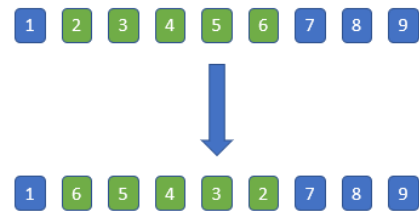


Figure 2.12: Inverse mutation operator

selected and their selection varies on the basis of the given optimization problem. Some of the most used stopping criteria are:

- Generations number
- Time limit
- Fitness limit
- Function tolerance
- Stall generations
- Stall time limit

Generations number criterium defines the maximum number of generations which can be generated. If this criterium is selected then the genetic algorithm stops when the number of generations reaches the maximum value. Fitness Limit criterium is the one which causes genetic algorithm stops when the value of the fitness function for the best point in the current population is less or equal to fitness limit. If function tolerance criterium is selected, the algorithm runs until the average relative change in the fitness function value is less than the tolerance. Stall generation is the criteria which if selected causes the algorithm stop when the average relative change in the fitness function value over Stall generations is less than Function tolerance. Lastly, Stall time limit and Time limit specify the time after that the algorithm is stopped and so prevent the algorithm from running too long. The algorithm stops as soon as one of these conditions is met. It is possible to specify the value of these criteria or use default ones.

2.9 Genetic Algorithm in MATLAB

MATLAB *MATrixLABoratory* is a high-performance language for technical computing that integrates different environments like computation, visualizations and programming [16]. It has many powerful built-in routines and other specific applications are collected in packages referred to a toolbox. There are toolboxes that have applications in many fields like:

- Signal processing
- Control theory
- Simulation
- Optimization and other fields of applied science and engineering.

In the case of this Master Thesis, the interesting is focused on the *optimization toolbox*. Global Optimization Toolbox provides functions in order to search global solutions to problems that can contain multiple maxima or minima. It includes various solvers as pattern search, genetic algorithm, multistate and global search in order to find the best solution for optimization problem where the objective or constraint function can be a generic one with different properties. Genetic algorithm toolbox, here considered, uses MATLAB matrix functions to build a set of versatile tools for implementing a wide range of genetic algorithm methods. The Genetic Algorithm Toolbox is a collection of routines, written mostly in m-file, which implement the most important functions in genetic algorithms. This type of algorithm can be exploited using the *ga* function which aims to find a local unconstrained minimum to the objective function. This function, in MATLAB environment, can be called using following syntax:

```
[x,fval,exitflag]=ga(fun, nvars A,b,Aeq,beq,lb,ub,nonlcon,options)
```

Parameters defined above have the following meaning:

- *x*: local unconstrained minimum. Best point that *ga* located during its iteration.
- *fval*: value of the objective function at *x*
- *fun*: objective function that describes the problem
- *exitflag*: reason that *ga* stopped, return as an integer value.
- *nvars*: number of design variables

- A, b : linear inequalities constraints ($Ax \leq b$) that describe the problem
- Aeq, beq : linear equalities constraints ($Aeqx \leq beq$)
- lb : lower bounds of the design variables
- ub : upper bounds of the design variables
- $nonlcon$: this function accepts x and return vectors C and Ceq , representing the non linear inequalities and equalities respectively. The function ga minimize fun such that $C(x) \leq 0$ and $Ceq(x) = 0$
- $options$: describes which optimization parameters are using to minimize the function. If $options$ is not specified default parametrs are used.

In next chapters this routine will be explain and it will be applied to solve an optimization problem relative to the determination of the best parking orbit during a Mars sample return mission.

2.10 Observation about Genetic Algorithm

Genetic algorithms accommodate all of the facets of soft computing, namely, robustness, non-linearity, and uncertainty. These characteristics permit this type of algorithm to have application in a lot of fields of study as optimization, parallelization, economics, neural network, robot trajectory optimization, machine learning and image processing. As computers continue to deliver accelerated performance, these applications will only become more routine. The flexibility of genetic algorithms to address general optimization problems using virtually any reasonable representation and performance index gives these techniques an advantage over classic numerical optimization procedures. Moreover, these algorithms offer a set of procedures that may be usefully applied to problems that have resisted solution by common techniques and can be hybridized with such techniques when such combinations appear beneficial In order to give a complete overview of these algorithms, advantages and disadvantages are here reported. The advantages of a genetic algorithm are:

- It is faster as compared to traditional method.
- It is more efficient as compared to traditional method.
- The search space is very large due to population diversity.
- It does not require any derivative informations.

- It provides not a single solution but a list of possible solutions.
- It can be used in order to solve multi-objective problems.

The disadvantages are:

- It is not suitable for all problems.
- Determination of fitness function is repeatedly performed which might be computationally expensive in some cases.
- Being stochastic, there are no guarantees on the optimality or the quality of the solution.
- It may not converge at the optimal solutions if they are not properly implemented.

Chapter 3

Physical Model

3.1 Two-Body Motion

The two-body motion is the first model that must be introduced. This model represents accurately the motion of artificial satellites, ballistic missiles or space probes orbiting around planets or the Sun can be studied and described. This method is based on the following three assumptions:

- The bodies are spherically symmetric. Thus, they are treated as point masses.
- The gravitational force is the only force acting on the system.
- The mass of the attracting mass must be much greater than orbiting body mass.

Let us consider the system of two bodies, m and M , illustrated in Fig 3.1. The motion of this system is governed by the following equation:

$$\ddot{\vec{r}} = -\frac{\mu}{r^3}\vec{r} \quad (3.1)$$

where:

- \vec{r} is the vector from M to m
- μ is the gravitational parameter of M

Equation (3.1), derived from Newton's Law of Universal Gravitation, can be used to introduce the concept of conservation of energy and conservation of angular momentum. These two parameters, defined as motion constants, make it possible to calculate the position and the velocity of the secondary body at any point in its orbit.

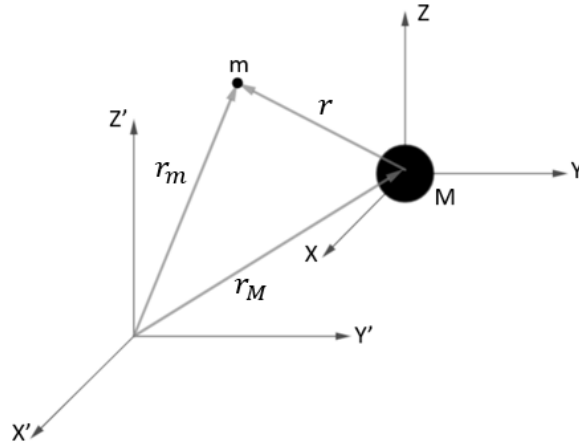


Figure 3.1: Relative motion of two bodies

3.1.1 Conservation of Mechanical Energy

The gravitational field in which the spacecraft goes is assumed to be conservative. Thus, from physics laws, is known that an object moving under the influence of gravity does not vary its mechanical energy but only exchange the kinetic and the potential energy. In orbit mechanics, the specific energy ϵ of a spacecraft is the quantity that remains constant along its orbit. This parameter is described by (3.2) where the first term represents the kinetic energy per unit mass while the second one the potential energy.

$$\epsilon = \frac{V^2}{2} - \frac{\mu}{r} \quad (3.2)$$

3.1.2 Conservation of Angular Momentum

The physics laws describe the gravitational force as a force directed radially toward the centre of the primary body so, the angular momentum of the spacecraft about the centre of the primary body reference frame does not change. In orbit mechanics, this constant of the motion is described by (3.3) and is called specific angular momentum.

$$\vec{h} = \vec{r} \times \vec{V} \quad (3.3)$$

From (3.3) must be observed that \vec{h} is the cross product of the spacecraft position vector and the velocity one so, it is always defined as perpendicular to the plane that contains these vectors. This plane, fixed in space, is called orbital plane. Now, introducing the flight path angle ϕ defined as

the angle between the velocity vector and the local horizontal plane, the scalar equation of the angular momentum can be described by (3.4).

$$h = rV \cos \phi \quad (3.4)$$

At the same time, if the complementary angle of ϕ is considered then the (3.4) can be rewritten by (3.5) where γ is defined as the zenith angle.

$$h = rV \sin \gamma \quad (3.5)$$

Zenith and flight path angle are shown in Fig.3.2

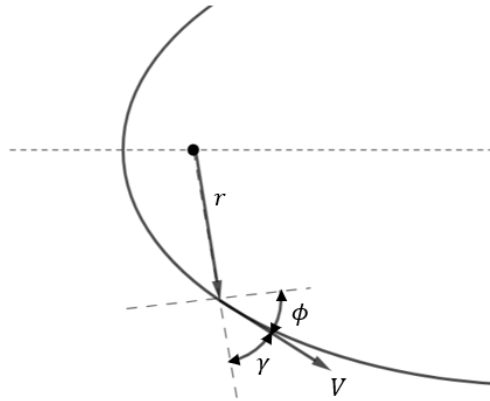


Figure 3.2: Flight Path Angle and Zenith Angle

3.2 Trajectory Equation and Conic Sections

3.2.1 Trajectory equations

As written before, the motion equation of a system composed of two bodies, where the attracting mass is much greater than orbiting body one, can be described by a differential equation expressed by (3.1). This one can be useful to obtain the trajectory equation that describes the orbit shape and its dimensions. Integrating (3.1), the polar equation of a generic conic section can be derived. It is expressed by:

$$r = \frac{h^2 / \mu}{1 + e \cos \nu} \quad (3.6)$$

where:

- h is the magnitude of the angular momentum

- μ is the gravitational parameter of the principal body
- e is the orbit eccentricity
- ν is the angle between the constant vector \hat{e} , directed from the central body to the periapsis, and the radius vector \vec{r} . It is called *true anomaly* and it is measured in the direction of the spacecraft motion.

Moreover, the equation of a conic section, written in polar coordinates with the origin located at a focus, can be introduced. It is expressed by (3.7) and permits to the (3.6).

$$r = \frac{p}{1 + e \cos \nu} \quad (3.7)$$

Thus, the following observations can be done:

- In the two-body problem the spacecraft moves along a conic section that has the primary body in its focus.
- The semi-latus rectum p of the trajectory is related to the angular momentum of the spacecraft
- The eccentricity of the conic section is the magnitude of the eccentricity vector \hat{e}

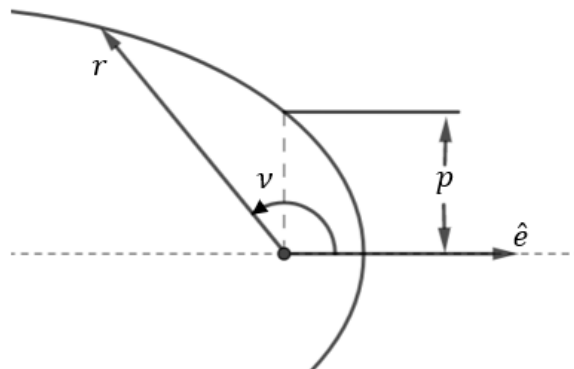


Figure 3.3: Generic conic section geometry

3.2.2 Conic Section

As written before, the family of curves called conic sections represents the only possible paths for an orbiting object in the two-body problem. When a spacecraft is under the influence of the

gravitational force of a primary body, it can travel along different types of orbits. These orbits, defined as Keplerian ones and represented in Fig 3.4, vary on the basis of their eccentricity value and can be summarized by the following list:

- Circular orbit: $e = 0$
- Elliptical orbit $0 < e < 1$
- Parabolic orbit $e = 1$
- hyperbolic orbit $e > 1$

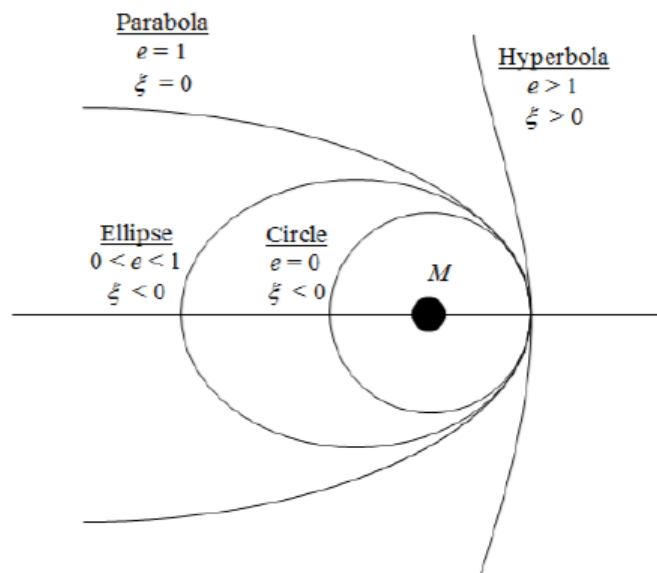


Figure 3.4: Types of keplerian orbits

Each conic section has two foci (F and F') due to its symmetrical conditions but, in orbital mechanics, only the first one has a great significance. It is the location of the primary body that permits to define some parameters. The first one is the *latus rectum*, indicated by $2p$ and defined as the width of each curve at the primary focus. The second one is the *major axis* described as the length of the chord passing through the foci. It is labelled $2a$ and it can be characterized by a positive, negative or infinity value. A positive major axis is obtained for circular and elliptical orbits while a negative value is defined for hyperbolic ones. Lastly, in the case of parabolic orbits, the semi-major axis has an infinite value. The third parameter that must be defined is the distance between the foci, indicated by $2c$. For circular orbits, foci are considered coincident and $2c$ is

zero, for the parabola $2c$ is infinite and for the hyperbola $2c$ is taken as negative. These three parameters just defined can be related through the following expressions:

$$e = \frac{c}{a} \tag{3.8}$$

$$p = a(1 - e^2) \tag{3.9}$$

The two extreme end-points of the major axis a are labelled as apses where the point farthest is defined apoapsis while the nearest one is called periapsis. The equation of these points can be easily derived from (3.7) inserting for the periapsis $\nu = 0^\circ$ and for the apoapsis $\nu = 180^\circ$. These equations are expressed by (3.10) and (3.11) respectively.

$$r_p = a(1 - e) \tag{3.10}$$

$$r_a = a(1 + e) \tag{3.11}$$

As written before the true anomaly is defined as the angle between the eccentricity vector that is direct toward the periapsis and the radius vector. The eccentricity vector expression is the (3.12) derived by the integration of the two-body equations.

$$\hat{e} = \frac{\vec{v} \times \vec{h}}{\mu} - \frac{\vec{r}}{r} \tag{3.12}$$

Lastly, an additional consideration about the specific orbital energy can be done. This constant of motion can be expressed as a function of the specific angular momentum in order to derive a new energy equation. This one is described by (3.13). It is valid for all conic orbits and tells that semi-major axis of an orbit depends only on the specific mechanical energy ϵ . Thus, depending on the semi-major axis value and then on the orbit types, the specific mechanical energy vary its sign.

$$\epsilon = -\frac{\mu}{2a} \tag{3.13}$$

The conic section properties are shown in Table 3.1.

Orbit shape	a	ϵ	e
Circular	> 0	< 0	0
Elliptical	> 0	< 0	< 1
Parabolic	∞	$= 0$	1
Hyperbolic	< 0	> 0	> 1

Table 3.1: Conic section properties

Equations above explained and described are referred to all types of conic sections. The attention will be now focused on the elliptical orbit and the hyperbolic one.

Elliptical Orbit

Elliptical orbits are the common ones. Planets orbits in the Solar System, as well as the Earth satellites, are ellipses. This conic section is represented in Figure 3.5 where are described its geometrical parameters. The first observation relative to this conic section is that the major axis is

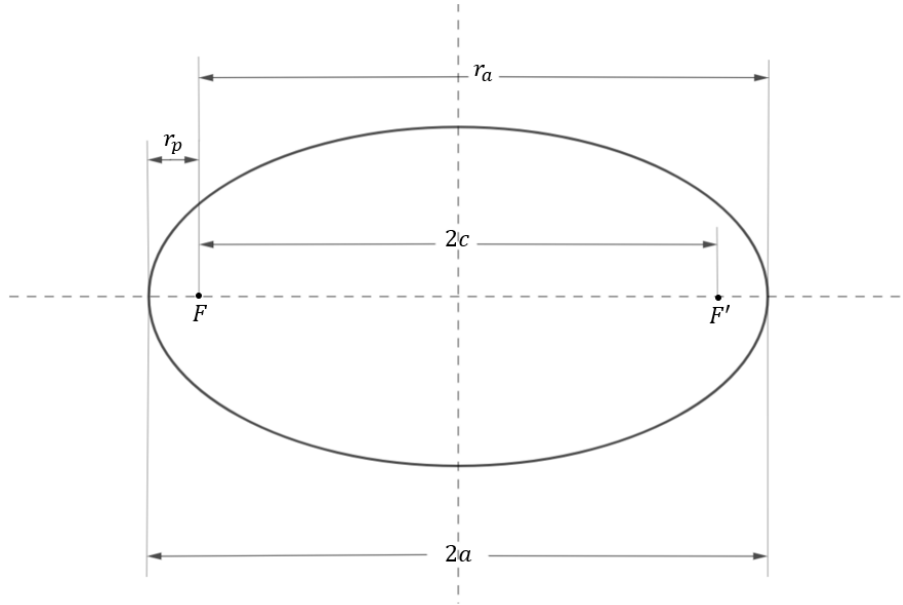


Figure 3.5: Elliptical orbit

the sum of the apoapsis and periapsis radius. This expression is described by (3.14). At the same time, the distance between foci can be defined by (3.15), as the difference between r_a and r_p .

$$r_p + r_a = 2a \quad (3.14)$$

$$r_a - r_p = 2c \quad (3.15)$$

Thus, the eccentricity can be expressed by:

$$e = \frac{r_a - r_p}{r_a + r_p} \quad (3.16)$$

Another important parameter that must be defined is the orbit period. This quantity depends only on the size of the orbit defined by the semi-major axis. This expression is described by (3.17).

$$\tau = 2\pi \sqrt{\frac{a^3}{\mu}} \quad (3.17)$$

Hyperbolic Orbit

Hyperbolic orbits are important if interplanetary missions are treated. During the capture, escape and fly-by phases within the planet sphere of influence, the spacecraft travels along this type of orbit. Moreover, a hyperbolic orbit is necessary if a probe must have some speed left over after it escapes from the planet's gravitational field. The geometry of this type of conic section is illustrated in Fig.3.6 where only the branch in which the motion is possible is represented.

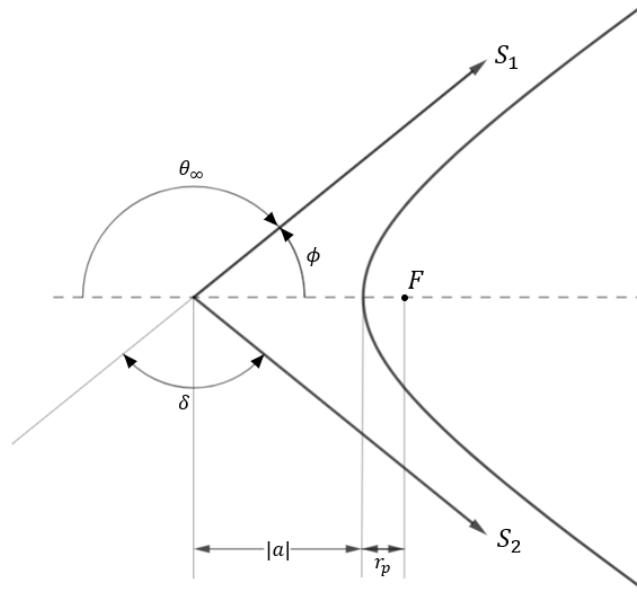


Figure 3.6: Hyperbolic orbit

The eccentricity is the first parameter that can be defined. This parameter is expressed by (3.18), where θ_∞ , i.e. the complementary angle of the true anomaly of the hyperbolic asymptotes ϕ , is taking into account.

$$e = -\frac{1}{\cos(180^\circ - \phi)} = -\frac{1}{\cos(\theta_\infty)} \quad (3.18)$$

Moreover, another expression for the eccentricity e can be defined. This expression is described by (3.20) and considers the angle between the asymptotes δ obtained by (3.19).

$$\delta = 180^\circ - 2\phi \quad (3.19)$$

$$e = \frac{1}{\sin(\delta/2)} \quad (3.20)$$

The second parameter to define is the hyperbolic excess speed that represents the velocity the body attains at as the distance tends to infinity. This parameter is important during the capture,

escape and fly-by phases. It can be derived from the energy equation written for two points on the hyperbolic escape trajectory. The first point is situated near the planet while the second one is located to an infinite distance. Thus, the expression of the hyperbolic excess speed is given by (3.21). Moreover, if the geometry of the hyperbola is known then another formulation can be exploited. This one is described by (3.22).

$$V_{\infty} = \sqrt{2 \left(\frac{V^2}{2} - \frac{\mu}{r} \right)} \quad (3.21)$$

$$V_{\infty} = \sqrt{-\frac{\mu}{a}} \quad (3.22)$$

3.3 Patched-Conic Approximation

The patched-conic approximation method allows for the two body-model of motion by patching together different conic sections. It assumes that at any instance in time, the spacecraft motion is solely influenced by the gravity of a single dominant body that defines the dominant region in which this force is applied. This region, defined as Sphere Of Influence (SOI) varies from planet to planet and depends on the mass ratio between the considered body and the Sun. The equation that describes the SOI radius is the (3.23) while SOI data for planets of the Solar System are shown in Table3.2.

$$r_{SOI} = R \left(\frac{m_{planet}}{M_{sun}} \right)^{2/5} \quad (3.23)$$

Thus, trajectories within the planet's sphere of influence are two body problems with the planet

Planet	Mass ratio (sun-planet)	r_{SOI}
Mercury	$6.0236 \cdot 10^6$	$1.12 \cdot 10^5$
Venus	$4.0852 \cdot 10^5$	$6.16 \cdot 10^5$
Earth	$3.3295 \cdot 10^5$	$9.25 \cdot 10^5$
Mars	$3.0987 \cdot 10^6$	$5.77 \cdot 10^5$
Jupiter	$1.0474 \cdot 10^3$	$5.46 \cdot 10^7$
Saturn	$3.4985 \cdot 10^3$	$5.18 \cdot 10^7$
Uranus	$2.2869 \cdot 10^4$	$8.68 \cdot 10^7$
Neptune	$1.9314 \cdot 10^4$	$1.51 \cdot 10^7$

Table 3.2: Planet's SOI with respect to the Sun

as the primary attracting body, and trajectories outside can be treated as two body problems with

the Sun as the primary attracting body. The entire Sample Return Mission, in according with the patched-conic approximation, can be divided into different phases:

- Earth planetocentric phase
- Heliocentric phase
- Mars planetocentric phase

The list above takes into account only the first leg of the mission. The return leg is the same as the first one but with reversed phases. In the Earth planetocentric phase, the launch is the most important operation. Its goal is to escape from Earth gravitational force in order to perform an interplanetary flight toward Mars. In the second phase, the spacecraft is under the Sun's gravitational force while in the third one the spacecraft enters inside the Mars Sphere Of Influence. Here, capture and escape manoeuvres are performed under the Mars's gravitational force. In this chapter, the attention is focused on the Mars planetocentric phase where the spacecraft performs the capture and the escape manoeuvres.

3.3.1 Planetocentric Phase

In according to the Mars Sample Return Mission, inside the Mars sphere of influence, the spacecraft will perform two types of manoeuvres:

- Parking orbit capture
- Parking orbit departure

During the first one, the spacecraft will leave the hyperbolic trajectory in order to insert itself into an elliptical/circular orbit while during the second one, the spacecraft will move from this orbit to a hyperbolic one. This phases are shown in Fig.3.7 and Fig.3.8.

3.3.2 Parking Orbit Capture

The first manoeuvre that the spacecraft must accomplish inside the Mars sphere of influence is the capture one (Fig.3.7). Thus, from its hyperbolic entry trajectory, it must move on a specific parking orbit. In order to perform this, a breaking manoeuvre must be executed and then, a velocity variation must be defined. The ΔV value can be calculated once the following data are known:

- Hyperbolic excess velocity or the energy level C_3 for the capture conditions

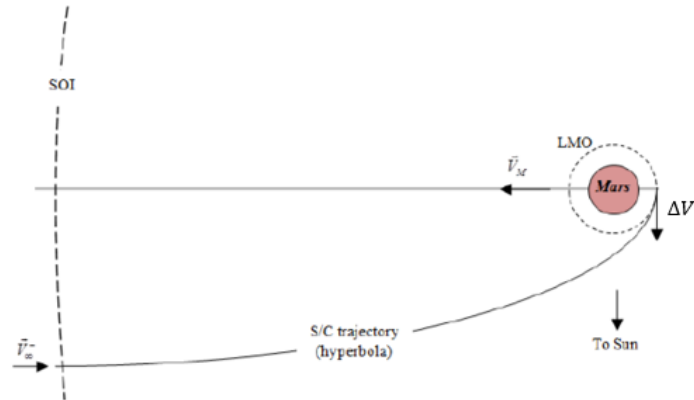


Figure 3.7: Capture manoeuvre - Mars SOI

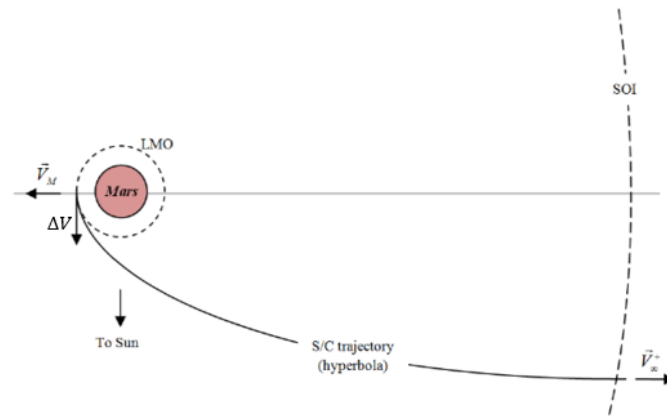


Figure 3.8: Escape manoeuvre - Mars SOI

- Capture Parking orbit velocity

The first parameter, described by V_∞ , is the velocity calculated by the patched-conic approximation method that links the heliocentric and planetocentric phases. Its value is assumed known thus, the energy of the hyperbola can be derived. This expression is described by (3.24).

$$\epsilon_\infty = \frac{V_\infty^2}{2} = \frac{C_3}{2} \quad (3.24)$$

Then, from the hyperbolic energy equation the expression of the hyperbolic velocity at a given radius can be derived. It is given by (3.25).

$$V_{hyperbola} = \sqrt{C_3 + \frac{2\mu}{r}} \quad (3.25)$$

The second parameter that must be evaluated is the parking orbit velocity. From the energy equation, knowing its geometry parameters, this expression can be derived. Parking orbit velocity for a given radius r is expressed by (3.26).

$$V_{orbit} = \sqrt{\frac{2\mu}{r} - \frac{\mu}{a}} \quad (3.26)$$

Thus, the velocity increment needed for the capture manoeuvre is given by (3.27) where V_{orbit} and $V_{hyperbola}$ are vector.

$$\Delta V_{capture} = V_{orbit} - V_{hyperbola} \quad (3.27)$$

3.3.3 Parking Orbit Departure

This subsection treats the escape manoeuvre (Fig.3.8) that will permit the spacecraft to transfer itself from the parking orbit to a hyperbolic one and then to escape from planet's sphere of influence. The first goal of this section is to relate the parking orbit conditions to the escape ones and then to determinate the velocity increment needed to perform the manoeuvre. The ΔV value can be calculated once the following data are known:

- Hyperbolic excess velocity or the energy level C_3 for the escape conditions
- Escape Parking orbit velocity

The calculation process is the same as the previous one related to the capture manoeuvre but the radius vector now considered is the escape one. Thus, equations described in the previous sections can be used. The velocity increment is described by (3.28) as the difference between the hyperbolic velocity and the parking orbit one.

$$\Delta V_{escape} = V_{hyperbola} - V_{orbit} \quad (3.28)$$

3.4 Hohmann Transfer

The Hohmann transfer is the most energy efficient two-impulse manoeuvre for transferring between two coplanar circular orbits sharing a common focus. The transfer orbit is an elliptical one, tangent to both circles at its apse line where the periapsis and apoapsis are the radii of the inner and outer circles. From Fig.3.9, representing the problem geometry can be quickly observed that the semimajor axis of the transfer orbit is given by the following equation:

$$a = \frac{r_1 + r_2}{2} \quad (3.29)$$

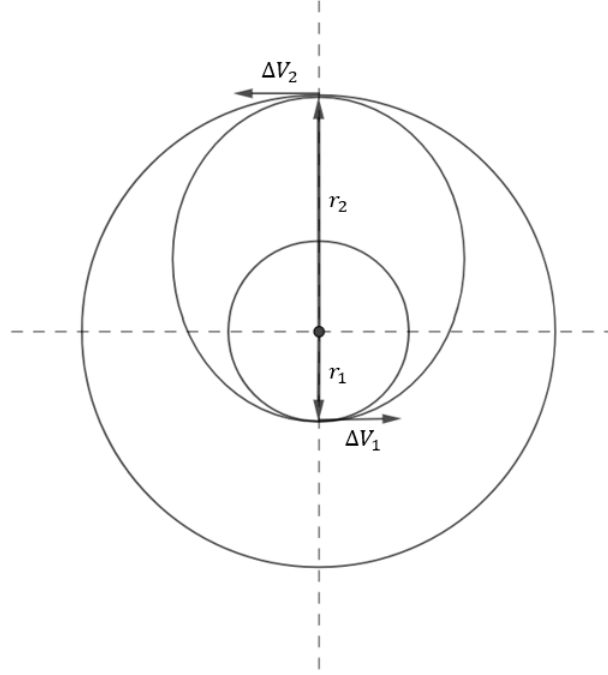


Figure 3.9: Hohmann Transfer

Hence, the energy of the transfer orbit is greater than the energy of the inner orbit ($a = r_1$), and smaller than the energy of the outer orbit ($a = r_2$). The velocities of the transfer orbit at periaapsis and apoapsis are given, from the conservation of energy equation, as:

$$V_{p-to} = \sqrt{2 \left(\frac{\mu}{r_1} - \frac{\mu}{r_1 + r_2} \right)} \quad (3.30)$$

$$V_{a-to} = \sqrt{2 \left(\frac{\mu}{r_2} - \frac{\mu}{r_1 + r_2} \right)} \quad (3.31)$$

The velocities of the inner and outer orbits are:

$$V_{inner} = \sqrt{\frac{\mu}{r_1}} \quad (3.32)$$

$$V_{outer} = \sqrt{\frac{\mu}{r_2}} \quad (3.33)$$

hence, the required impulses at perigee and apogee are:

$$\Delta V_1 = V_{p-to} - V_{inner} = \sqrt{\frac{\mu}{r_1}} \left(\sqrt{\frac{2r_2}{r_1 + r_2}} - 1 \right) \quad (3.34)$$

$$\Delta V_1 = V_{outer} - V_{a-to} = \sqrt{\frac{\mu}{r_2}} \left(1 - \sqrt{\frac{2r_1}{r_1 + r_2}} \right) \quad (3.35)$$

If the initial orbit has a radius larger than the final orbit, the same strategy can be followed but in this case, negative impulses will be required, first at apoapsis and then at periapsis, to decelerate the satellite. This manoeuvre can be performed from an elliptical orbit to another one, but in this case, the velocity for the circular orbits must be replaced with the elliptical one. Ascent and descent phases from and to the Mars surface can be modeled by this type of manoeuvre.

Descent Manoeuvre

A one-impulsive model is exploited for the descent phase, where the spacecraft travels from the parking orbit to the Mars Surface. Thus, the velocity increment to perform the descent manoeuvre is given by the following equation:

$$\Delta V_{descent} = V_{po} - V_{to} \quad (3.36)$$

where V_{po} is the velocity at the periapsis point of the stopover orbit while V_{to} is the velocity of the Hohmann transfer orbit at its apoapsis point. In this case, the Hohmann transfer orbit is characterized by a semimajor axis given by:

$$a = \frac{r_{p-po} + r_{Mars}}{2} \quad (3.37)$$

Ascent Manoeuvre

The ascent phase is treated as a sequence of three different manoeuvres. The Mars Ascent Vehicle starts the ascent phase moving on a transfer orbit in order to reach a desired apex h from the Mars surface. Knowing the angle between these two positions (described by vectors), transfer orbit parameters can be defined and then, the orbit energy and the velocities along this orbit may be evaluated. In particular, the velocities at r_{Mars} and $r_1 = r_{Mars} + h$ are given by:

$$V_1 = \sqrt{2\epsilon + 2\frac{\mu}{r_{Mars}}} \quad (3.38)$$

$$V_2 = \sqrt{2\epsilon + 2\frac{\mu}{r_{Mars} + h}} \quad (3.39)$$

where the first velocity is also the first velocity increment that must be performed $\Delta V_1 = V_1$. From the desired apex h , the Mars Ascent vehicle will move on a Hohmann transfer orbit characterized by a major axis equal to $r_1 + r_{p-po}$ in order to reach the periapsis of the parking orbit. Knowing

this parameter, the energy of the Hohmann transfer orbit and then, the two velocities needed for the determination of the velocity increments can be defined. Then, the velocity increments for these two manoeuvres are defined by:

$$|\Delta V_2| = |V_{H-h}| - |V_2| \quad (3.40)$$

$$|\Delta V_3| = |V_{H-p-po}| - |V_{p-po}| \quad (3.41)$$

where:

- V_{H-h} is the Hohmann transfer orbit velocity at the apex h
- V_{H-p-po} is the Hohmann transfer orbit velocity at the periapsis of the stopover orbit
- V_{p-po} is the parking orbit velocity at its periapsis point

Lastly, the total velocity increment for the entire ascent phase can be defined. This parameter is given by:

$$|\Delta V_{ascent}| = 1.1|\Delta V_1| + |\Delta V_2| + |\Delta V_3| \quad (3.42)$$

where losses are taken into account on the first manoeuvre.

Chapter 4

Parking Orbit Optimization Problem

4.1 Problem Definition

During the design process of a Mars Sample Return mission or a future manned one, the parking orbit selection is one of the most crucial phases. The definition of this orbit involves a detailed study of different factors that can directly influence the complexity, the total cost and the scientific goals that must be achieved. The parking orbit selection can be defined as an optimization process, where each phase must be taken into account for the global mission success and the minimization of its cost. If this one is not properly performed, other mission phases can be affected by the wrong stopover orbit choice and then, the total cost can increase. Moreover, the stopover orbit selection must include a detailed trade-off study where different factors should be considered [19]. The most important ones are:

- Science Mission constraints
- Landing site accessibility requirements
- Mission performance
- Perturbations

Each factor listed above have a significant function inside the mission design, but in this section, the focus is on the mission performance. This parameter can be described by the ΔV budget that represents the sum of all the velocity increment performed in a mission. This factor immediately affects the total mission cost, because, a velocity variation implies a propellant consumption. Moreover, the cost of a single manoeuvre can be expressed as a function of the burn position that determines misalignment losses. In fact, from spaceflight mechanical laws can be derived that

an injection manoeuvre in a wrong position causes a ΔV penalty with subsequent increase of the propellant consumption. The task of this chapter is to describe an optimization algorithm that aims to minimize the total velocity increments defining the best parking orbit orientation given data for capture and escape phases. The baseline paper is "*Optimum Parking Orbit Orientation for a Three-Dimensional Capture-Escape Mission*" [20] that describes the problem through the following statement: **"To determine the orientation of the stopover orbit and the capture and escape injections positions that will minimize the velocity increments"**.

4.2 Assumptions

In general, the entire problem may take place in the three-dimensional space where no-coplanar conditions are defined. These conditions are the real one and, in this case, the entire problem is a function of time. Thus, the orientation of the hyperbolas for capture and escape manoeuvres and the parking orbit can change due to the perturbations resulting from the planet's oblateness.

- Two-body mechanics is used for capture, stopover orbit and escape conditions. Thus, the spacecraft is treated as a point mass.
- The orientation of approach/escape hyperbola and its energy level are defined by the arrival, stay and departure time.
- The stopover orbit can be circular or elliptical and may have any orientation.
- Each manoeuvre is characterized by a single-impulsive burn. Thus the entire problem can be studied as two-impulsive burn problem.
- Stay time in stopover orbit around Mars is limited to a fraction of the planet's orbital period.

4.3 Input & Output Definition

The optimization algorithm here treated is referred to three different Mars Sample return phases. These are:

- Capture
- Stopover orbit selection
- Escape

Each one occurs within the Mars sphere of influence then only the gravitational force of the Red Planet is considered. Arrival and departure conditions are defined by the energy level C_3 and the direction of the hyperbolic excess speed. This last parameter is described by Right Ascension and Declination angles. On the other hand, the stopover orbit is defined by its geometrical parameters, i.e. eccentricity, semi-major axis and inclination. These parameters are summarized in Table 4.1.

Input Data	Description	UM
a	Parking orbit semi-major axis	km
e	parking orbit eccentricity	/
i	Parking orbit inclination	$^\circ$
α_c	Right Ascension - Capture conditions	$^\circ$
δ_c	Declination - Capture conditions	$^\circ$
C_{3c}	Energy level - Capture conditions	km^2/s^2
α_e	Right Ascension - Escape conditions	$^\circ$
δ_e	Declination - Escape conditions	$^\circ$
C_{3e}	Energy level - Escape conditions	km^2/s^2

Table 4.1: Optimization problem input parameters

Thanks to input data, the optimization algorithm can generate results. These ones are related to the minimization of the total velocity increment then they are referred to:

- manoeuvres ΔV
- manoeuvres positions
- Stopover orbit orientation

The first two terms are referred to capture and escape impulsive-burn and are defined by the angular position respect to the ascending node and by the velocity increment (or decrement) that permits to execute these manoeuvres. Moreover, the total ΔV is calculated by the sum of the capture and escape contributions. Lastly, the stopover orbit orientation is defined by two orbital parameters that are the Argument of Periapsis and the Right Ascension of the Ascending Node. These two parameters and the two manoeuvres positions are not properly defined as output because the genetic algorithm takes these one as input data and during the calculation process provides their optimization. The output and the optimized variables are summarized in Table 4.2.

Optimized Variables	Description	UM
ρ_c	Injection position vector - Capture conditions	°
ρ_e	Injection position vector - Escape conditions	°
Ω_c	Right Ascension of the Ascending Node - Capture conditions	°
ω_c	Argument of Periapsis - Capture conditions	°
Ω_e	Right Ascension of the Ascending Node - Escape conditions	°
ω_e	Argument of Periapsis - Escape conditions	°
Output Data	Description	UM
ΔV_c	Total Velocity increment - Capture conditions	km/s
ΔV_e	Total Velocity increment - Escape conditions	km/s
ΔV	Total Velocity increment	km/s

Table 4.2: Optimization problem output parameters and optimized variables

The assumptions before listed describe the problem as a function of time then, output data can vary from capture to escape conditions. This happens in the case where perturbations due to planet's oblateness are not neglected. In the opposite case, the orientation of the stopover orbit does not vary with time then the Right Ascension of the Ascending Node and the Argument of Periapsis for capture and escape conditions coincide.

4.4 Reference Systems

The entire problem evolves into the Mars sphere of influence where two inertial reference systems can be defined. These are:

- Mars equatorial reference frame
- Orbital reference frame

The Mars equatorial reference frame is defined by $\hat{I}\hat{J}\hat{K}$ axes. It is oriented such that \hat{I} axis points towards the vernal equinox and the \hat{K} axis is normal to the equatorial plane. Thus, \hat{J} can be defined as the axis which completes the counterclockwise system. The second one is referred to the orbital plane where the spacecraft lies in the time between the manoeuvres and is defined by $\hat{\xi}\hat{\eta}\hat{\zeta}$ axes. It has the $\hat{\xi}$ axis in the stopover orbit plane along the line of ascending node, the $\hat{\zeta}$ axis along the angular momentum vector of the orbit and then the $\hat{\eta}$ axis completes the counterclockwise reference system. These reference systems are shown in Fig.4.1 and Fig.4.2. In the last one the problem geometry is also described and angles described in Table 4.1 and 4.2 are illustrated. Moreover, from Fig.4.2 vector relations between inertial reference systems and other vector quantities may

be observed. These relations are governed by the product of different rotations about the axes of an inertial reference system. These rotations are defined by three different matrices where the rotation angle is positive if the rotation is in the counter-clockwise direction when viewed by an observer looking along the axis towards the origin. These matrices are described by the following equations where a generic reference system characterized by 1,2,3 axes is considered:

$$R_1(\alpha) = \begin{bmatrix} 1 & 0 & 0 \\ 0 & \cos \alpha & -\sin \alpha \\ 0 & \sin \alpha & \cos \alpha \end{bmatrix} \quad (4.1)$$

$$R_2(\beta) = \begin{bmatrix} \cos \beta & 0 & \sin \beta \\ 0 & 1 & 0 \\ -\sin \beta & 0 & \cos \beta \end{bmatrix} \quad (4.2)$$

$$R_3(\gamma) = \begin{bmatrix} \cos \gamma & -\sin \gamma & 0 \\ \sin \gamma & \cos \gamma & 0 \\ 0 & 0 & 1 \end{bmatrix} \quad (4.3)$$

In next sections the following writing convention is adopted:

- $[\alpha]_i$ indicates a positive rotation of α angle about the i axis.
- $[-\alpha]_i$ indicates the inverse of the rotation matrix $[\alpha]_i$ about the i axis.

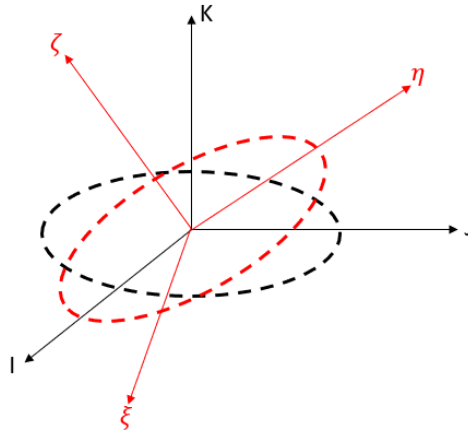


Figure 4.1: Inertial reference systems - Optimization problem

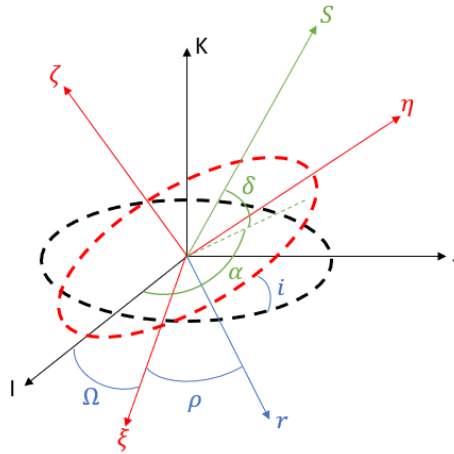


Figure 4.2: Noncoplanar stopover orbit launch window geometry

4.5 Calculation Process

This calculation process treats the problem with the assumption that perturbations due to planet's oblateness are neglected. Thus, the orientation of the stopover orbit is assumed constant then it does not vary with time. At the end of the algorithm discussion, a paragraph will be dedicated to the perturbative problem where perturbations equations will be described. The attention is now focused on the non-perturbative problem which can be divided into three different phases:

- Stopover orbit definition
- Capture and escape conditions determination
- Total velocity increment determination

4.5.1 Stopover Orbit Definition

This subsection concerns the determination of the following stopover orbit parameters for both capture and escape conditions:

- Spacecraft injection position vector
- Spacecraft injection velocity vector

In this discussion, these vector quantities will be defined in reference to $\hat{I}\hat{J}\hat{K}$ system then rotation matrix described by (4.1)-(4.3) will be used.

The first parameter to obtain is the vector along the line of the ascending node, defined by (4.4).

It can be solely defined only when the orbit plane inclination is not zero, otherwise the orbit plane and the equatorial one coincide and then this vector is not univocally defined. Moreover, in this case, Ω and ω lie in the same plane.

$$\hat{A} = [\Omega_c]_K [i]_I \begin{bmatrix} 1 \\ 0 \\ 0 \end{bmatrix} \quad (4.4)$$

The position of the spacecraft along the parking orbit is defined by the True Anomaly, labelled by v . This parameter, expressed by (4.5), is the angle measured in the motion direction between the periapsis of the stopover orbit and the position vector. Thus, knowing this parameter and using the polar equation of the elliptic orbit, the magnitude of the position vector can be defined. This expression is given by (4.6).

$$v = 2\pi + \rho_c - \omega_c \quad (4.5)$$

$$r = \frac{a(1 - e^2)}{1 + e \cos v} \quad (4.6)$$

The position vector can be defined only after the definition of its direction. Thus, its unit vector must be established. This one is described by (4.7) as the result of a sequence of three different rotations about \hat{K} - \hat{I} - \hat{K} axes.

$$\hat{r} = [\Omega_c]_K [i]_I [\rho_c]_K \begin{bmatrix} 1 \\ 0 \\ 0 \end{bmatrix} \quad (4.7)$$

Then the position vector is univocally defined by the following equation:

$$\vec{r} = r\hat{r} \quad (4.8)$$

Spaceflight mechanics laws determine that the spacecraft velocity depends on its position so, it is characterized by a different velocity value in each point of the orbit. Thus, knowing the position vector, the velocity one can be derived. Its magnitude, given by (4.9), is obtained from the specific mechanical energy of the stopover orbit calculated through the knowledge of its geometrical data. Instead, the velocity unit vector can be established only after the introduction of the flight path angle. In this case, this parameter is defined as the angle between the spacecraft radial direction and the velocity one. The angle γ is represented in Fig.4.3 and it can be derived from the specific angular momentum. This last parameter is described by (4.10) while the flight path angle is given by (4.11).

$$V = \sqrt{\mu \left(\frac{2}{r} - \frac{1}{a} \right)} \quad (4.9)$$

$$\begin{cases} \vec{h} = \vec{r} \times \vec{V} \Rightarrow h = rV \sin \gamma \\ h = \sqrt{\mu a (1 - e^2)} \end{cases} \quad (4.10)$$

$$\gamma = \sin^{-1} \left(\frac{h}{rV} \right) \quad (4.11)$$

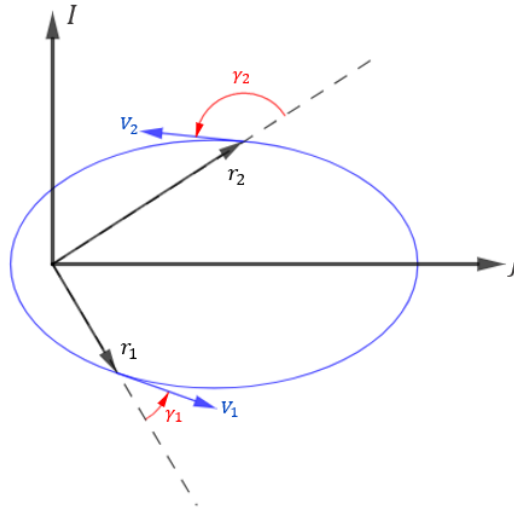


Figure 4.3: Stopover orbit geometry and flight path angle definition

Lastly, before to start the velocity vector calculation, some logic considerations about the flight path angle have to be done. This angle is derived from the inverse sine function, that is defined within the range of $[-\pi/2, \pi/2]$, and also is related to the true anomaly. Thus, in order to properly execute the calculation process, the following logic considerations have to be inserted inside the algorithm:

$$\begin{cases} 0 \leq \gamma \leq \pi/2 \text{ for } 0 \leq (\rho_c - \omega) \leq \pi \\ \pi/2 < \gamma < \pi \text{ for } \pi < (\rho_c - \omega) < 2\pi \end{cases} \quad (4.12)$$

All the parameters needed for the unit vector calculation are now defined so this parameter can be determined. This expression is given by (4.13).

$$\hat{V} = [\Omega_c]_K [i]_I [\rho_c]_K [\gamma]_K \begin{bmatrix} 1 \\ 0 \\ 0 \end{bmatrix} \quad (4.13)$$

Moreover, the velocity vector is defined by the following equation:

$$\vec{V} = V\hat{V} \quad (4.14)$$

At this point, all the parameters for the stopover orbit are defined. Thus, the next step is to determine the capture and escape conditions along the hyperbolic trajectories.

4.5.2 Capture And Escape Conditions Determination

This section describes which is the process that must be followed in order to obtain the optimal conditions for capture and escape manoeuvres in terms of hyperbolic parameters. Thus, given capture and escape conditions, this section analyzes which are the possible hyperbolic trajectories and which are the best points of these hyperbolas to perform capture and escape manoeuvres. This points will be evaluated in terms of velocity then two parameters will be defined:

- Hyperbolic velocity for the capture manoeuvre
- Hyperbolic velocity for the escape manoeuvre

As written before, capture and escape conditions are assigned. They are defined by three parameters that permit to establish the hyperbolic excess velocity vector, labelled by \vec{V}_∞ . These are:

- Energy level C_3
- Right ascension of hyperbolic asymptote α
- Declination of hyperbolic asymptote δ

The first parameter is related to the V_∞ magnitude while the second one and the third one permit to define the V_∞ unit vector. This unit vector for both manoeuvres, also representing the direction of the hyperbolic asymptote, is the first parameter to define. It is characterized by three components along the axes of the equatorial reference system and is obtained by a sequence of two rotations

around \hat{I} and \hat{J} axes. This expression is given by (4.15) while the three components of the unit vector are described by (4.16).

$$\hat{S} = [\alpha]_I [-\delta]_J \begin{bmatrix} 1 \\ 0 \\ 0 \end{bmatrix} \quad (4.15)$$

$$\hat{S} = \begin{bmatrix} \cos \alpha \cos \delta \\ \sin \alpha \cos \delta \\ \sin \delta \end{bmatrix} \quad (4.16)$$

In order to give a clear problem explanation, capture and escape manoeuvres are now treated separately.

Capture conditions

As written before when the spacecraft goes inside the Mars sphere of influence its trajectory is a hyperbola that is characterized by a hyperbolic asymptote defined by (4.16). When the spacecraft performs the capture burn, its trajectory changes and it moves into an elliptical or circular orbit. In this situation, the position vector is fixed and then two angles, between this vector and the hyperbolic asymptote, are determined. These ones, labelled by β_1 and β_2 are defined by the following equations:

$$\beta_1 = \cos^{-1} \left(\frac{\hat{S} \cdot \hat{r}}{|\hat{S}| |\hat{r}|} \right) \quad (4.17)$$

$$\beta_2 = 2\pi - \cos^{-1} \left(\frac{\hat{S} \cdot \hat{r}}{|\hat{S}| |\hat{r}|} \right) \quad (4.18)$$

These angles are calculated using the convention that β is positive when it is measured in the direction of motion along the hyperbola from \hat{S} to \hat{r} . Moreover, these two solutions involve that for each outgoing or incoming asymptote and a fixed position vector, two hyperbolas with different eccentricity, which satisfy the asymptote direction and the energy level, can be constructed. These ones, using the convention above explained, are characterized by two types of motion defined on the basis of the direction of the hyperbolic angular momentum \hat{W}_h . In particular:

- Motion is called *direct* when $\hat{W}_h \cdot \hat{K} > 0$
- Motion is called *retrograde* when $\hat{W}_h \cdot \hat{K} < 0$

The hyperbolic angular momentum direction can be evaluated defining its unit vector that also establishes the orientation of the plane of the hyperbola. In this case, using the convention that a positive angle is measured in the counterclockwise direction, this parameter can be derived by (4.19). The direction of the angular momentum is then function of β angle that defines, on the basis of its value, the sign of the components of \hat{W}_h .

$$\hat{W}_h = \frac{(\hat{S} \times \hat{r})}{\sin \beta} \quad (4.19)$$

The two hyperbolas, derived by the definition of two β angles, can be characterized by any orientations in the three-dimensional space. Thus, in order to define this orientation, the true anomaly of the hyperbolic asymptote and then the hyperbolic periapsis vector, for both hyperbolas, must be defined. The ϕ_A calculation process is based on the following step:

- Determination of the ϕ_A tangent
- Calculation of the hyperbola eccentricity
- determination True anomaly of the hyperbolic asymptote

The first one is given by (4.21) where σ is established by the following equation as a function of the position of the spacecraft and the energy level of the hyperbola:

$$\sigma = \frac{C_3 r}{2\mu} \quad (4.20)$$

$$\tan \phi_A = \sigma \sin \beta + \sqrt{(1 + \sigma)^2 - (1 + \sigma \cos \beta)^2} \quad (4.21)$$

The second step permits to define the eccentricity of the hyperbola given by the β value. This expression is a function of the true anomaly of the hyperbolic asymptote above defined, and it can be defined by (4.22).

$$e_h = \sqrt{\tan^2 \phi_A + 1} \quad (4.22)$$

Lastly, the third step permits to define the ϕ_A angle. The equation here used is derived from the hyperbola geometry and is a function of its eccentricity. This expression is the following one:

$$\phi_A = \cos^{-1} \left(-\frac{1}{e_h} \right) \quad (4.23)$$

A further verification of the value obtained from (4.23) can be then easily executed reversing the equation (4.21). In this case, some logic considerations must be taken into account because the inverse tangent function is defined between $-\pi/2$ and $\pi/2$ but β values must be included between 0 and 2π .

Knowing the position of the periapsis of the hyperbola (determined by ϕ_A) and the angle between the asymptote and the injection position vector, the true anomaly of the spacecraft on the hyperbola is univocally defined. This angle, labelled by ν_{hyp} , is the equivalent of the true anomaly of the stopover orbit and then is defined as the angle between the periapsis and the injection position vector. The relation of this angle with ϕ_A and β is the following one:

$$\nu_{hyp} = \phi_A - \beta \quad (4.24)$$

The problem geometry, in reference to the angles above defined, is illustrated in Figure 4.4 where for a better view a coplanar problem is considered.

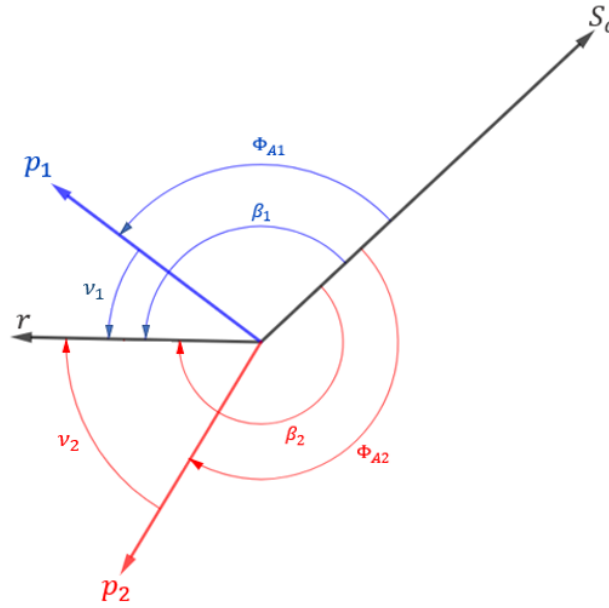


Figure 4.4: Geometry for two possible solutions for the capture manoeuvre

Once the position of the spacecraft on the hyperbola is determined, its velocity vector can be defined. This expression is given by the following equation:

$$\vec{V}_h = V_h \hat{V}_h \quad (4.25)$$

The velocity magnitude is defined as in the previous case where the specific energy equation was taken into account. This equation is given by (4.26) as a function of two different points on the hyperbola. The first one is the manoeuvre point while the second one is an infinite one.

$$V_h = \sqrt{\frac{2\mu}{r} + C_3} \quad (4.26)$$

The velocity unit vector is defined by (4.27) where it can be noted the introduction of the flight path angle.

$$\hat{V}_h = \hat{r} \cos \gamma_h + (\hat{W}_h \times \hat{r}) \sin \gamma_h \quad (4.27)$$

As for the section above, but in this case for the hyperbolic trajectory, this angle can be evaluated through the definition of the angular momentum. The determination process the flight path angle is the following one:

$$\left\{ \begin{array}{l} \vec{h}_h = \vec{r} \times \vec{V}_h = rV_h \sin \gamma_h \hat{W}_h \\ h_h = \mu \sqrt{\frac{e_h^2 - 1}{C_3}} \end{array} \right. \quad (4.28)$$

$$\gamma_h = \sin^{-1} \left(\frac{h_h}{rV_h} \right) \quad (4.29)$$

The introduction of the flight path angle permits to add an additional logic consideration. In fact, observing equation (4.24), it can be easily observed that the injection manoeuvre can be accomplished on either the incoming or the outgoing leg of the hyperbola. Therefore, the flight path angle γ_h is dependent upon the angle ϕ and this relation can be traduced by means of the following logic consideration:

$$\left\{ \begin{array}{l} 0 \leq \gamma_h \leq \pi/2 \text{ for } 0 \leq \phi \leq \pi \\ \pi/2 < \gamma_h < \pi \text{ for } \pi < \phi < 2\pi \end{array} \right. \quad (4.30)$$

Lastly, an additional verification concerning the position vector can be done. The entire calculation process is correct only if the hyperbola position vector coincides to the stopover orbit one when the capture manoeuvre is performed. Thus, the result of the equation (4.6) must coincide with the result of the following equation:

$$r_h = \frac{a_h (e_h^2 - 1)}{1 + e_h \cos v_{hyp}} \quad (4.31)$$

where a_h is the semi-major axis of the hyperbola that can be defined by (4.32).

$$a_h = \frac{\mu}{C_3} \quad (4.32)$$

Escape conditions

The escape manoeuvre consists of an impulsive burn that permits the spacecraft to leave the parking orbit and then to move on a hyperbolic trajectory leaving the Mars sphere of influence. Escape conditions are assigned, so the calculation process must define which is the best point of the orbit to execute the impulsive-burn in terms of position and velocity. In this case, some conventions change with respect to the previous one. As before, when the position vector is fixed β angles can be determinate. They are expressed by the following equations, with the assumption that they are positive when measured in the direction of motion along the escape hyperbola from \hat{r} to \hat{S} :

$$\beta_1 = \cos^{-1} \left(\frac{\hat{r} \cdot \hat{S}}{|\hat{r}||\hat{S}|} \right) \quad (4.33)$$

$$\beta_2 = 2\pi - \cos^{-1} \left(\frac{\hat{r} \cdot \hat{S}}{|\hat{r}||\hat{S}|} \right) \quad (4.34)$$

These two solutions involve the presence of two hyperbolas characterized by different eccentricity values. Moreover, from the convention above defined, can be deduced that the motion of these two hyperbolas is different and then, if the first one is direct, the second one is retrograde. Thus, also the angular momentum change. This constant of motion, for escape manoeuvre, is defined by (4.34).

$$\hat{W}_h = \frac{(\hat{r} \times \hat{S})}{\sin \beta} \quad (4.35)$$

The determination of the true anomaly of the injection position vector v_{hyp} and the orientation angle of the asymptote ϕ_A are all related and depend upon the orientation of the plane of the hyperbola. Thus, knowing the unit vector of the angular momentum, these two angles can be determined. The process is the same as the one described in the above section, but the equation that permits to calculate $\tan \phi_A$ is different. This process is described by (4.36)-(4.40) while the relationships between angles are represented in Fig.4.5.

$$\sigma = \frac{C_3 r}{2\mu} \quad (4.36)$$

$$\tan \phi_A = -\sigma \sin \beta - \sqrt{(1 + \sigma)^2 - (1 + \sigma \cos \beta)^2} \quad (4.37)$$

$$e_h = \sqrt{\tan^2 \phi_A + 1} \quad (4.38)$$

$$\phi_A = \cos^{-1} \left(-\frac{1}{e_h} \right) \quad (4.39)$$

$$v_{hyp} = \phi_A - \beta \quad (4.40)$$

At this point, in order to properly define the hyperbolic velocity vector for the escape manoeuvre, the flight path angle γ_h must be defined. This parameter can be evaluated using equations described in the section above. These equations, defined by (4.28)-(4.29) must be associated to the same logic considerations about β and γ_h . Moreover, the hyperbolic velocity magnitude can be defined by (4.26), through the same considerations about the specific orbital energy of the capture hyperbola. Lastly, the unit vector of the hyperbolic velocity vector can be determined by (4.27) and then the hyperbolic escape velocity can be evaluated by the product of its magnitude and its unit vector.

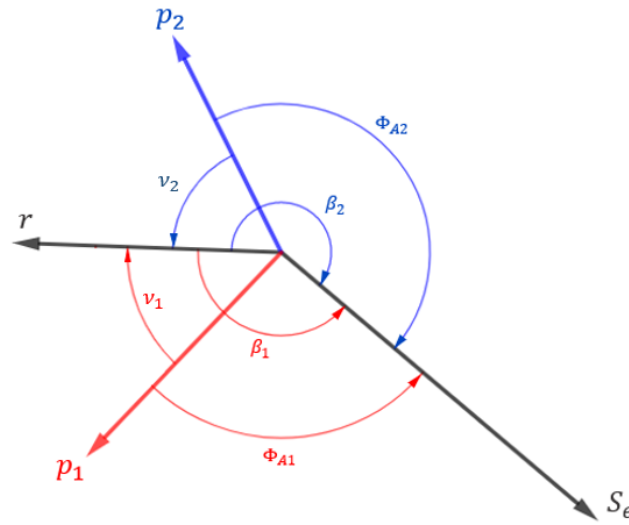


Figure 4.5: Geometry for two possible solutions for the escape manoeuvre

4.5.3 Total Velocity Increments Determination

This section concerning the total velocity increment determination defined, from the algorithm statement, as the parameter to minimize. The goal of this section is to define the relationships that permit to derive the total cost of the manoeuvres given:

- Stopover orbit velocity at capture position
- Hyperbolic velocity at capture position
- Stopover orbit velocity at escape position
- Hyperbolic velocity at escape position

Remembering that the entire problem is treated as composed of two impulsive-burn then the total cost can be defined by the sum of two contributions where the first one is relative to the capture manoeuvre while the second one is relative to the escape one. Thus, this parameters can be defined by the following equation:

$$\Delta V_{tot} = \Delta V_c + \Delta V_e \quad (4.41)$$

The next paragraphs will treat the determination of the cost for the capture and escape manoeuvres.

Capture ΔV Determination

The capture manoeuvre is defined as a braking one, where the spacecraft decreases its velocity in order to move on the stopover orbit. The velocity variation can be defined by the following equation:

$$\Delta V_c = \sqrt{V_{hc}^2 + V_c^2 - 2V_c V_{hc} (\hat{V}_c \cdot \hat{V}_{hc})} \quad (4.42)$$

Escape ΔV Determination

The second manoeuvre executed by the spacecraft is the escape one that permits to move from the stopover orbit to a hyperbolic trajectory and then to leave the Mars Sphere of Influence. In this case, a positive velocity variation is performed so this manoeuvre is defined as an accelerating one. The velocity increment is then defined by the following equation:

$$\Delta V_e = \sqrt{V_{he}^2 + V_e^2 - 2V_e V_{he} (\hat{V}_e \cdot \hat{V}_{he})} \quad (4.43)$$

4.6 Perturbations Determination

This section treats the optimization problem in the case which perturbations due to the planet's oblateness are not neglected, then the orientation of the stopover orbit changes in the time between the capture and the escape manoeuvres. Thus, this variation is a function of the stopover orbit time that causes the variation of the following orbital parameters:

- Argument of Periapsis ω
- Right ascension of the ascending node Ω

The laws governing the variation of these two parameters are the following ones:

$$\Omega_e = \Omega_c + \dot{\Omega} (JD_e - JD_c) \quad (4.44)$$

$$\omega_e = \omega_c + \dot{\omega} (JD_e - JD_c) \quad (4.45)$$

where the time is defined by the Julian calendar while the subscripts c and e are referred to capture and escape condition respectively. Moreover, derivatives on time of the Right Ascension of the Ascending node and the Argument of Periapsis can be determined by the following equations:

$$\dot{\Omega} = -\tau \cos i \left[3 \left(\frac{K_2}{p^2} \right) + 10 \left(\frac{K_2}{p^4} \right) (1 + 1.5e^2) (1 - 1.75 \sin^2 i) \right] \quad (4.46)$$

$$\dot{\omega} = \tau \left[3 \left(\frac{K_2}{p^2} \right) (1 - 1.5 \sin^2 i) + 10 \left(\frac{K_4}{p^4} \right) (1 + 0.75e^2) (1 - 5 \sin^2 i + 4.375 \sin^4 i) \right] - \dot{\Omega} \cos i \quad (4.47)$$

where:

$$p = a(1 - e^2) \quad (4.48)$$

$$\tau = \sqrt{\frac{\mu}{a^3}} \quad (4.49)$$

$$K_2 = \frac{703656}{\tau^2} \quad (4.50)$$

$$K_4 = \frac{225170}{\tau^2} \quad (4.51)$$

From the equations above reported some considerations can be done:

- For short stay times $\dot{\Omega}\Delta t \simeq 0$ and $\dot{\omega}\Delta t \simeq 0$. Thus, RAAN and LAAN do not vary with time. In this case, perturbations caused by planet's oblateness can be neglected.
- The Argument of periapsis derivative over time is a function of $\dot{\Omega}$. Thus, a Ω variation involves a ω variation if the inclination of stopover orbit is not $\pi/2$ or $\pi/2 + k\pi$.
- Perturbations are not always the cause for a ΔV increment. In certain conditions, they can permit to decrease the total velocity increment and the to save propellant. These conditions are not here treated but they can be a future case of study.

4.7 Algorithm Implementation

The optimization problem above defined and explained can be solved by using the optimization toolbox of the MATLAB environment. This toolbox provides different solver to optimize the variables of a certain objective function and then to minimize the same one. In this case, *genetic algorithm* solver is used to optimize the total velocity increment optimizing the following four variables:

- Argument of Periapsis of the stopover orbit ω
- Right Ascension of the Ascending Node of the stopover orbit Ω
- Capture injection ρ_c
- Escape injection position ρ_e

These one are the input variables of the genetic algorithm while the objective function is defined by a MATLAB function containing the code of the algorithm above explained. This one has the following syntax:

```
function [DeltaV]=ParkingOrbit(x)
```

where:

- DeltaV is the parameter to optimize
- ParkingOrbit is the name of the objective function
- x is the vector which contains the problem variables

Lastly, the solver `ga` can be invoked in MATLAB environment using the following syntax:

```
[OptPar,DeltaV]=ga(@ParkingOrbit,4,[],[],[],[],LB,UB,[],options)
```

where:

- `optPar` is the solution vector which contains the best values that `ga` locates during its iterations
- `DeltaV` is the objective function value at the solution `optPar`
- 4 is the variables number
- `LB` is the lower bound of the variables. In this case, it is equal to `[0 0 0 0]`
- `UB` is the upper bound of the variables. In this case, it is equal to `[2π 2π 2π 2π]`
- `options` contains the optimization parameters different from default ones.

In order to give a clear overview of the genetic algorithm implemented via MATLAB the Fig.4.6 is here reported.

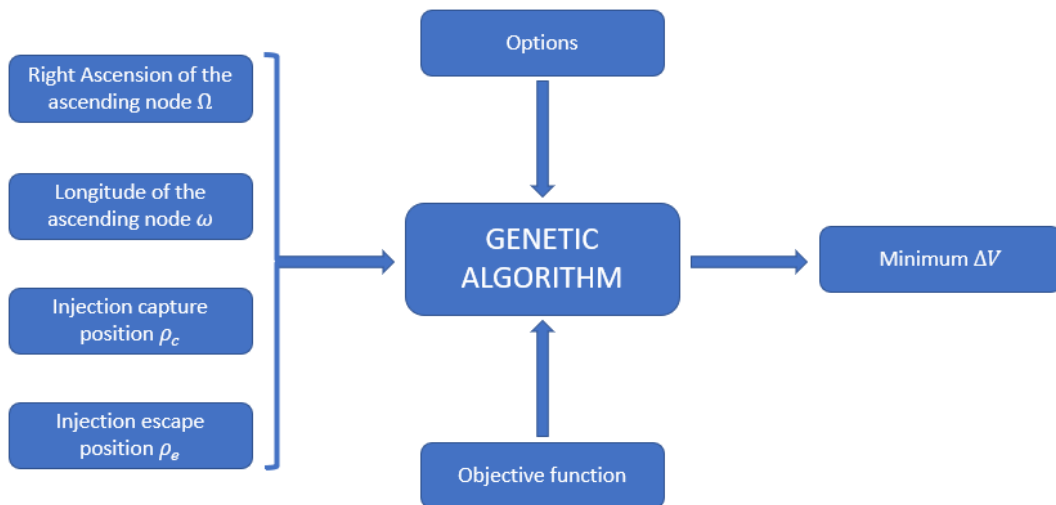


Figure 4.6: Description of the algorithm implemented via MATLAB

Chapter 5

Results

This chapter aims to study and observe the results obtained by the optimization algorithm considering different study cases. The first one will be relative to a coplanar problem, where the solution is well known. Here, in order to test the efficiency of the algorithm, the computational solution will be compared to the analytical one. Subsequently, other cases characterized by different starting conditions will be treated. Non-coplanar manoeuvres will be considered and then, an application for a future Mars Return Mission will be studied. Lastly, the study of the parking orbit geometry variation will be treated and two different cases will be considered. The first one will consider only the capture and escape manoeuvres while the second one will treat even the descent and ascent phases.

5.1 Direct Coplanar problem

The optimization algorithm, treated in the previous chapter, is here used to solve a test problem where the solution is well-known. Considering a coplanar and symmetrical problem, the algorithm accuracy and efficiency will be evaluated in comparison with the analytical solution.

5.1.1 Test problem definition

The problem here described aims to minimize the total velocity increment considering the following assumptions:

- Coplanar conditions for both capture and escape manoeuvres
- Elliptical stopover orbit
- Same energy level for capture and escape conditions

- Symmetrical Right Ascension values for capture and escape conditions
- Zero declination values for capture and escape conditions
- Non-perturbative problem
- Periapsis of the elliptic orbit selected to allow for a solution where it is coincident with the hyperbola periapses

The assumptions listed above make it possible to treat the problem as a bi-dimensional one evolving on the $\hat{I}\hat{J}$ plane (Fig.5.1). In accordance with spaceflight mechanics laws, with these conditions, both manoeuvres are executed at the periapsis of the hyperbolas that coincide with the stopover orbit one. These conditions are desirable but, in general, these coplanar relationships are not always satisfied due to the dynamic nature of the relative geometry of the hyperbolic asymptotes and the parking orbit. In fact, if perturbations due to planet's oblateness are not neglected, this relative geometry changes and thus, the coplanar problem cannot be considered. The assumptions listed above permit to define the input data for the problem. They are shown in Table 5.1 and are referred to the case where the true anomaly of the hyperbolic asymptote (θ_∞), for both capture and escape manoeuvres, is assumed to be equal to 45° .

Input Data	Description	value	UM
a	Parking orbit semi-major axis	20000	km
e	Parking orbit eccentricity	0.8	/
i	Parking orbit inclination	0	$^\circ$
α_c	Right Ascension - Capture conditions	45	$^\circ$
δ_c	Declination - Capture conditions	0	$^\circ$
C_{3c}	Energy level - Capture conditions	4.435	km^2/s^2
α_e	Right Ascension - Escape conditions	-45	$^\circ$
δ_e	Declination - Escape conditions	0	$^\circ$
C_{3e}	Energy level - Escape conditions	4.435	km^2/s^2

Table 5.1: Input data - Direct Coplanar problem

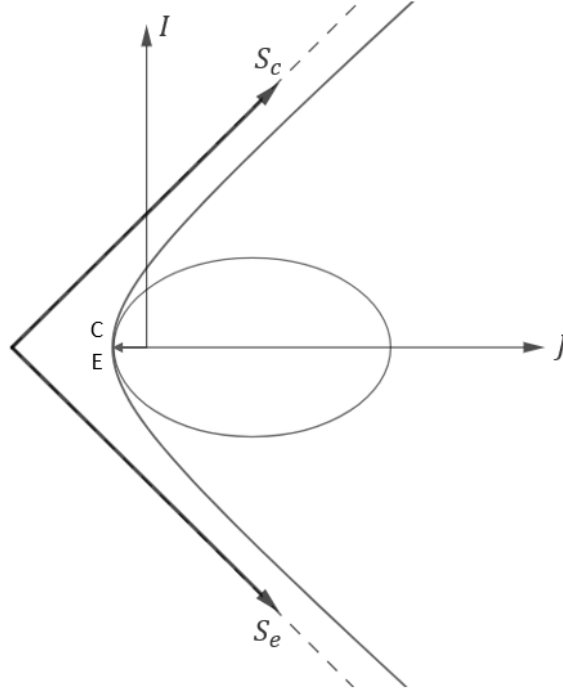


Figure 5.1: Coplanar problem geometry

5.1.2 Analytical solution

As written before, the problem defined above is characterized by a well-known solution where both capture and escape burns are performed at the hyperbolas periapsis that coincides to the stopover orbit one. In this case, the stopover orbit orientation is fixed by the following equation:

$$\omega + \Omega = 180^\circ \quad (5.1)$$

This solution, in terms of total velocity increment, may also be simply evaluated analytically by the following calculation process:

1. Determination of the stopover periapsis speed

Knowing the geometry data of the stopover orbit and then the periapsis distance, the periapsis speed can be easily calculated by the energy equation. This velocity is given by the following equation:

$$V_{orbit} = \sqrt{\frac{2\mu}{r_p} - \frac{\mu}{a}} \quad (5.2)$$

2. Determination of the speed of the hyperbola

The manoeuvres are performed to the periapsis of the hyperbolas then the spacecraft speed

before the capture/escape burn can be evaluated matching the energy equation considering the periapsis point and an infinite distance one (where the speed is known from C_3). The desired velocity equation, relative to the periapsis point of the hyperbola, is the following one:

$$V_{hyp} = \sqrt{\frac{2\mu}{r_p} + V_\infty^2} \quad (5.3)$$

3. Determination of the manoeuvre velocity increment

The velocity increment can be evaluated as the difference between the hyperbolic velocity and the stopover orbit velocity where both are evaluated at the periapsis of the respective orbits. This equation for capture and escape maneuvers is given by:

$$\Delta V_{capt} = V_{orbit} - V_{hyp-capt} \quad (5.4)$$

$$\Delta V_{esc} = V_{hyp-esc} - V_{orbit} \quad (5.5)$$

4. Determination of the total velocity increment

The total velocity increment can be calculated by the sum of the capture and escape contributions. Thus, the calculation process described above have to be followed for both manoeuvres. The equation of the total velocity increments is given by:

$$\Delta V_{tot} = |\Delta V_{capt}| - |\Delta V_{esc}| \quad (5.6)$$

The calculation process here explained was used in order to determinate the total velocity increment considering the input data reported in Table 5.1. The results obtained are shown in Table 5.2, where, through its observation, some considerations can be done. These are:

- The capture and the escape velocity increments are the same due to the symmetrical conditions of the problem.
- The velocity increment for the capture manoeuvre is negative. Thus, this manoeuvre is defined as a breaking one where the spacecraft decreases its velocity to move into the parking orbit.
- The velocity increment for the escape manoeuvre is positive then, the spacecraft performs an accelerating manoeuvre to move into the escape hyperbola.

Results	Value	UM
r_p	4000	<i>km</i>
V_{orbit}	4.3901	<i>km/s</i>
$V_{hyp_{capt}}$	5.0842	<i>km/s</i>
ΔV_{capt}	-0.6941	<i>km/s</i>
$V_{hyp_{esc}}$	5.0842	<i>km/s</i>
ΔV_{esc}	0.6941	<i>km/s</i>
ΔV_{tot}	1.3882	<i>km/s</i>

Table 5.2: Results of the analytical study.

5.1.3 Computational solution

This subsection concerns the study of the coplanar and symmetrical problem by means of the optimization algorithm implemented in MATLAB. This algorithm exploits the ga solver of the MATLAB optimization toolbox to determinate the best orientation of the parking orbit and the position of the capture and escape manoeuvres minimizing the total velocity increment. Thus, the optimization process concerns four variables:

- Right Ascension of the Ascending Node (Ω)
- Argument of Periapsis (ω)
- Angle between the ascending node and the capture injection point in stopover orbit (ρ_c)
- Angle between the ascending node and the escape injection point in stopover orbit (ρ_e)

Moreover, in order to improve the efficiency and the accuracy of the calculation process the following optimization options were set:

- Selection process: Tournament
- Number of Elite individuals: 4
- Crossover fraction: 0.3
- Initial population range: $[0, 2\pi]$
- Search space: $[0, 2\pi]$ for each variable

Thanks to these options and input data (Table 5.1), the algorithm has been generated the results reported in Table 5.3. These results are referred to the two possible solutions in terms of hyperbolic

trajectories calculated from the hypothesis that, for a fixed position vector and for a specific hyperbolic asymptote, two hyperbolas, characterized by different types of motion, can be constructed. The first solution, which is also the minimum one, is characterized by a direct motion that is the same of the stopover orbit one (Fig.5.3 and Fig.5.4), while the second one (Fig.5.5 and Fig.5.6) evolves in a retrograde motion and then, is more expensive in terms of propellant consumption. This confirms that the optimum injection manoeuvre occurs when the direction of motion on the hyperbola is the same of the stopover orbit one. In the first solution the velocity increment corresponds to the analytical one and the stopover orbit orientation coincide with the one assumed for the same case (the sum of the Right Ascension of the Ascending Node and Argument of Periapsis is a multiple of 180°). Moreover, the injection position vectors for capture and escape manoeuvres coincide to the periapsis vector. Thus, the calculation process can be considered correct and then the algorithm too. Lastly, an observation relative to the calculation speed and then the efficiency of the algorithm can be done. The algorithm speed can be evaluated observing the Fig.5.2 where the fitness function is plotted respect to the generations number. The calculation process quickly converged in about 70 generations when the best solution was founded and then, the mean fitness value and the best one coincided. This number is lower than the maximum one, i.e. 400, then the convergence of the algorithm was really fast.

Results	Solution 1	Solution 2	UM
ΔV_{capt}	0.6941	8.7571	<i>km/s</i>
ΔV_{esc}	0.6941	8.7571	<i>km/s</i>
ΔV_{tot}	1.3882	17.5142	<i>km/s</i>
ω	332.17	332.17	$^\circ$
Ω	207.83	207.83	$^\circ$
ρ_c	332.12	332.12	$^\circ$
ρ_e	332.14	332.14	$^\circ$
e_c	1.4142	1.2247	/
e_e	1.4142	1.2247	/
$\vec{V}_{orbit-c}$	[0, -4.3901, 0]	[0, -4.3901, 0]	<i>km/s</i>
$\vec{V}_{orbit-e}$	[0, -4.3901, 0]	[0, -4.3901, 0]	<i>km/s</i>
\vec{V}_{hyp-c}	[0, -5.0842, 0]	[-3.5951, 3.5951, 0]	<i>km/s</i>
\vec{V}_{hyp-e}	[0, -5.0842, 0]	[3.5951, 3.5951, 0]	<i>km/s</i>
\vec{W}_{h-c}	[0, 0, 1]	[0, 0, -1]	/
\vec{W}_{h-e}	[0, 0, 1]	[0, 0, -1]	/

Table 5.3: Results for the direct coplanar problem

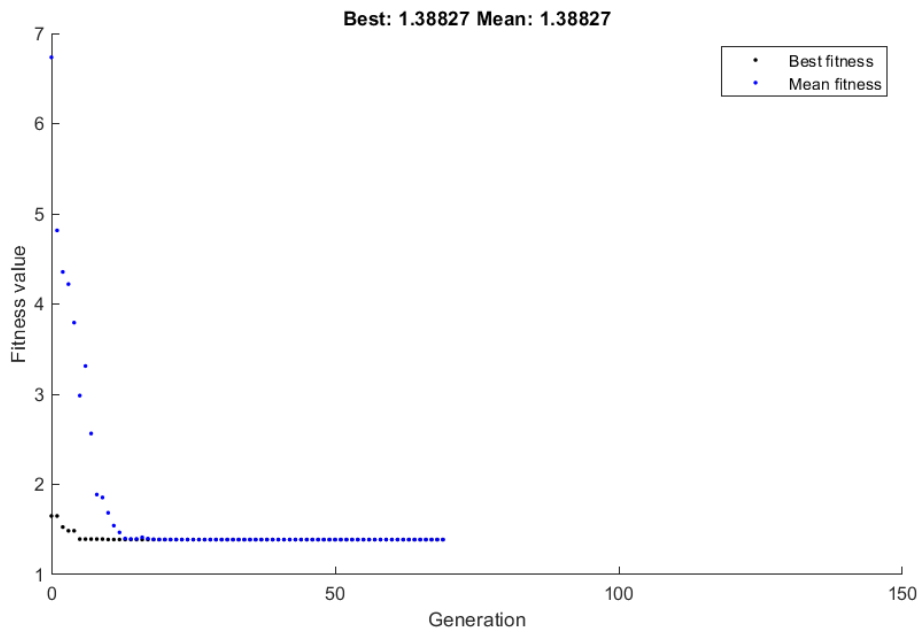


Figure 5.2: Fitness value-Generation plot for the coplanar and symmetrical problem

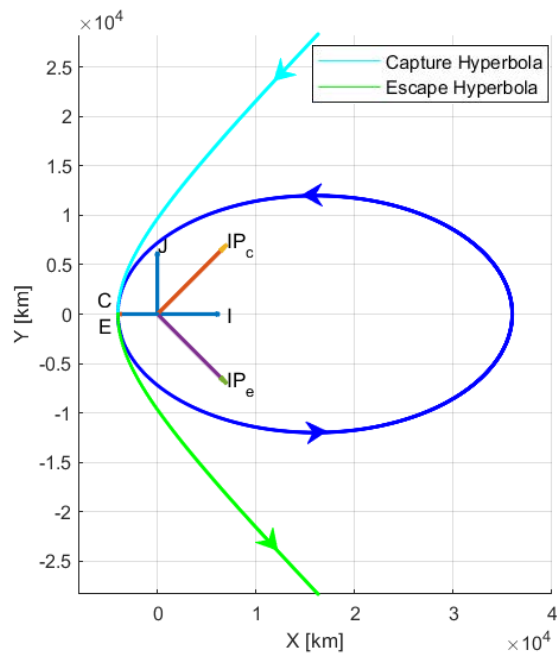


Figure 5.3: Direct and coplanar problem: First Solution

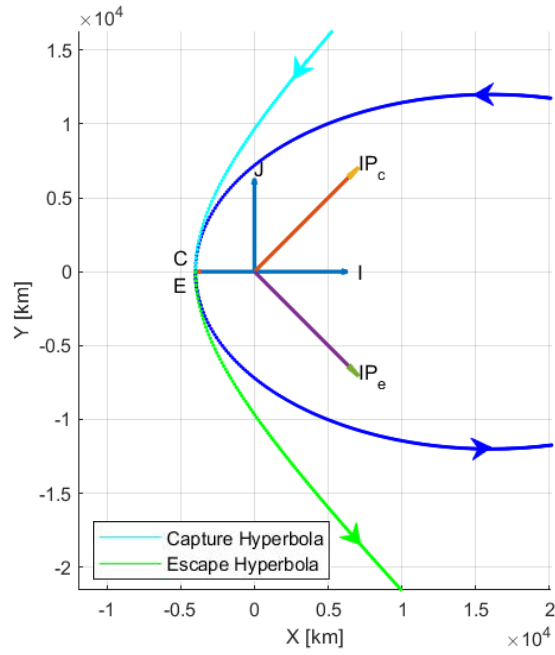


Figure 5.4: Direct and coplanar problem: First Solution - Zoom

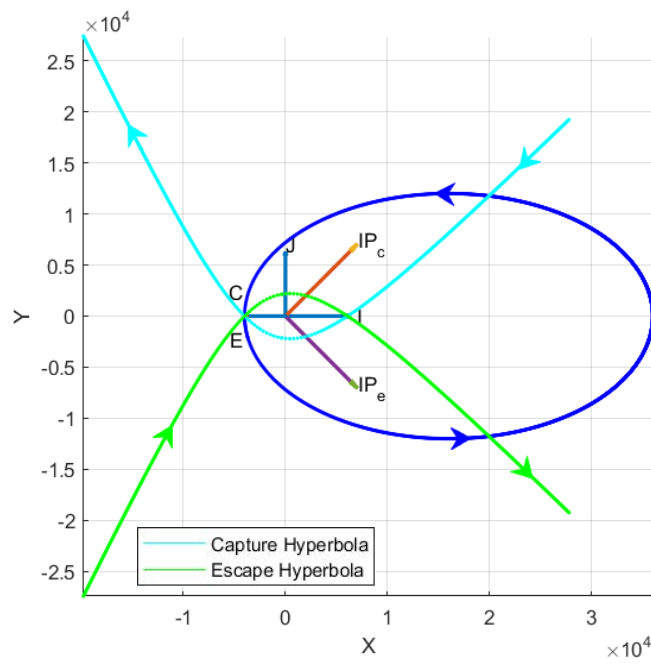


Figure 5.5: Direct and coplanar problem: Second Solution

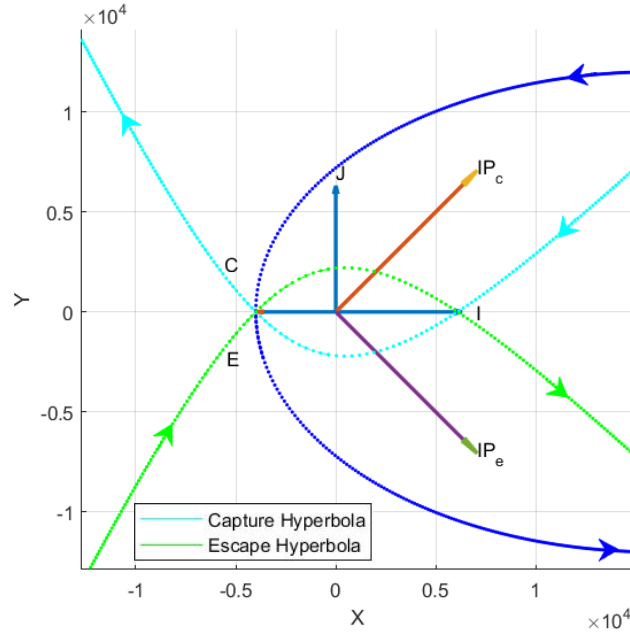


Figure 5.6: Direct and coplanar problem: Second Solution - Zoom

5.2 Retrograde Coplanar problem

This section aims to verify the algorithm accuracy when retrograde conditions are assigned. The problem is always considered as coplanar so, the parking orbit inclination is supposed to be equal to 180° . Moreover, in order to make a comparison to the direct one, starting conditions for capture and escape hyperbolas are exchanged. Input data for this problem are summarized in Table 5.4.

Input Data	Value	UM
a	20000	km
e	0.8	/
i	180	$^\circ$
α_c	-45	$^\circ$
δ_c	0	$^\circ$
C_{3c}	4.435	km^2/s^2
α_e	45	$^\circ$
δ_e	0	$^\circ$
C_{3e}	4.435	km^2/s^2

Table 5.4: Input data - Retrograde Coplanar problem

The results, obtained exploiting the same optimization options of the previous problem, are shown in Table 5.5. Moreover, the problem geometry plot, generated by MATLAB, is here reported. Fig.5.7 and Fig.5.8 show the first solution while Fig.5.9 and Fig.5.10 the second one.

The total velocity increment is equal to the one referred to the direct problem but, in this case, the entire motion is retrograde ($\hat{W}_{hz} < 0$). Thus, the difference is the type of motion and then the general direction of the velocities. In fact, if Table 5.3 and Table 5.5 are compared, it can be easily observed as the velocities relative to the stopover orbit and capture/escape hyperbolas are characterized by opposite direction. Moreover, as in the direct problem, the optimum injection manoeuvres occur when the direction of the motion in the hyperbola is in the same as the motion in the stopover orbit. Lastly, it can be observed as the orientation of the stopover orbit coincides with the direct case one, in fact, the sum of the Right Ascension of the Ascending node and the Argument of Periapsis is a multiple of 180° . These results demonstrate as the algorithm can be considered correct even for retrograde conditions.

Results	Solution 1	Solution 2	UM
ΔV_{capt}	0.6941	8.7571	km/s
ΔV_{esc}	0.6941	8.7571	km/s
ΔV_{tot}	1.3882	17.5142	km/s
ω	355.49	355.49	°
Ω	207.83	207.83	°
ρ_c	355.5	355.5	°
ρ_e	355.5	355.5	°
e_c	1.4142	1.2247	/
e_e	1.4142	1.2247	/
$\vec{V}_{orbit-c}$	[0, 4.3901, 0]	[0, 4.3901, 0]	km/s
$\vec{V}_{orbit-e}$	[0, 4.3901, 0]	[0, 4.3901, 0]	km/s
\vec{V}_{hyp-c}	[0, 5.0842, 0]	[-3.5951, -3.5951, 0]	km/s
\vec{V}_{hyp-e}	[0, 5.0842, 0]	[3.5951, -3.5951, 0]	km/s
\hat{W}_{h-c}	[0, 0, -1]	[0, 0, 1]	/
\hat{W}_{h-e}	[0, 0, -1]	[0, 0, 1]	/

Table 5.5: Results for the retrograde coplanar problem

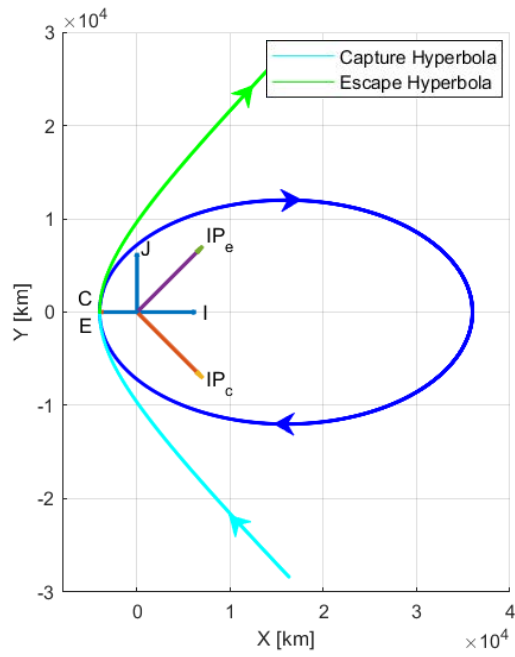


Figure 5.7: Retrograde and coplanar problem: First Solution

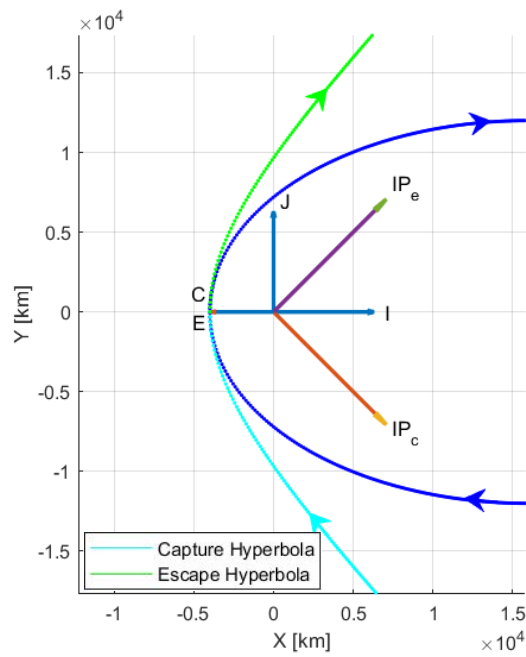


Figure 5.8: Retrograde and coplanar problem: First Solution - Zoom

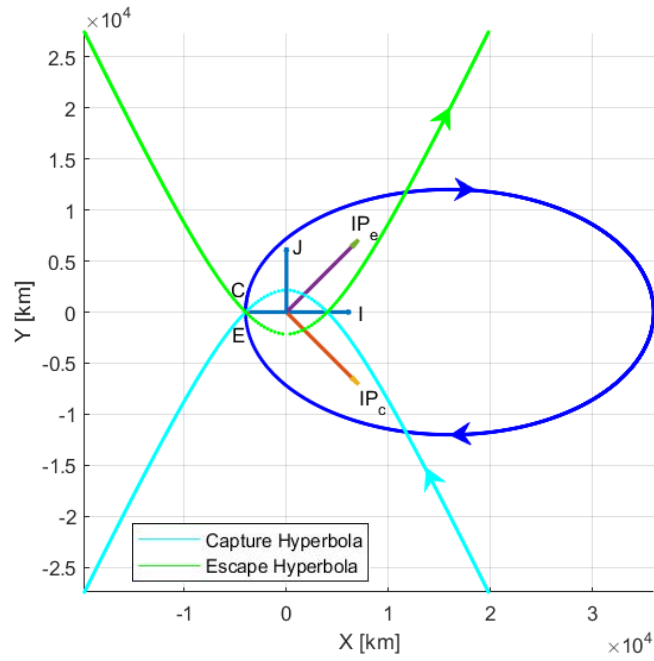


Figure 5.9: Retrograde and coplanar problem: Second Solution

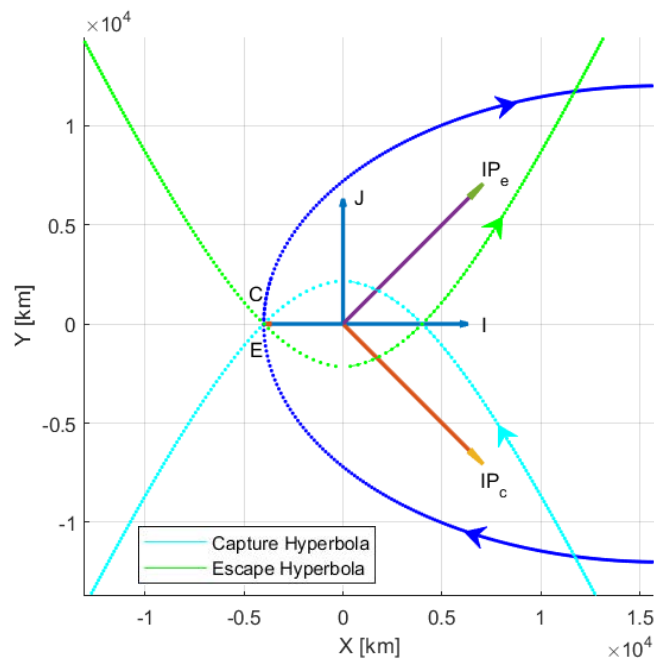


Figure 5.10: Retrograde and coplanar problem: Second Solution - Zoom

5.3 Right Ascension Variation

This section treats the coplanar, symmetrical problem when the Right Ascension of the hyperbolic asymptotes vary while the energy level is fixed. Thus, the optimization algorithm results will be studied for the following conditions:

- Identical rotation for capture and escape hyperbolic asymptotes
- Not identical rotation for capture and escape hyperbolic asymptotes

5.3.1 Identical rotation for capture and escape hyperbolic asymptotes

This paragraph treats the coplanar and symmetrical problem when the Right Ascension of capture and escape hyperbolic asymptotes varies of the same value. Thus, the angle among them is fixed. Considering the input data shown in Table 5.6, two study cases characterized by different right ascension values will be analyzed. These are:

1. $\alpha_c = 90^\circ - \alpha_e = 0^\circ$
2. $\alpha_c = 270^\circ - \alpha_e = 180^\circ$

Input Data	value	UM
a	20000	km
e	0.8	/
i	0	$^\circ$
δ_c	0	$^\circ$
C_{3c}	4.435	km^2/s^2
δ_e	0	$^\circ$
C_{3e}	4.435	km^2/s^2

Table 5.6: Input data - Right Ascension variation

1. $\alpha_c = 90^\circ - \alpha_e = 0^\circ$

This first study case aims to analyze the coplanar and symmetrical problem with a positive rotation of 45° . The optimized variables and the output data, generated by the ga solver, are shown in Table 5.7 while the problem geometry obtained by MATLAB is illustrated in Fig.5.11. From Table 5.7, it can be observed that the total velocity increment is equal to the one referred to the case where $\alpha = 45^\circ$ and $\alpha = -45^\circ$ because of the same starting conditions in terms of energy level and the angle between the capture and escape asymptotes. This angle permits to generate hyperbolas that satisfy the energy level imposed as input datum where capture and escape manoeuvres are performed to their periapsis. Moreover, it can be noted as the velocities of capture/escape hyperbolas and stopover orbit are characterized by the same direction. This condition permits to have the minimum velocity increment.

Results	Value	UM
ΔV_{capt}	0.6941	km/s
ΔV_{esc}	0.6941	km/s
ΔV_{tot}	1.3882	km/s
ω	317.27	°
Ω	87.73	°
ρ_c	317.27	°
ρ_e	317.27	°
e_c	1.4142	/
e_e	1.4142	/
$\vec{V}_{orbit-c}$	[3.104, -3.104, 0]	km/s
$\vec{V}_{orbit-e}$	[3.104, -3.104, 0]	km/s
\vec{V}_{hyp-c}	[3.595, -3.595, 0]	km/s
\vec{V}_{hyp-e}	[3.595, -3.595, 0]	km/s
\hat{W}_{h-c}	[0, 0, 1]	/
\hat{W}_{h-e}	[0, 0, 1]	/

Table 5.7: Results for $\alpha_c = 90^\circ - \alpha_e = 0^\circ$

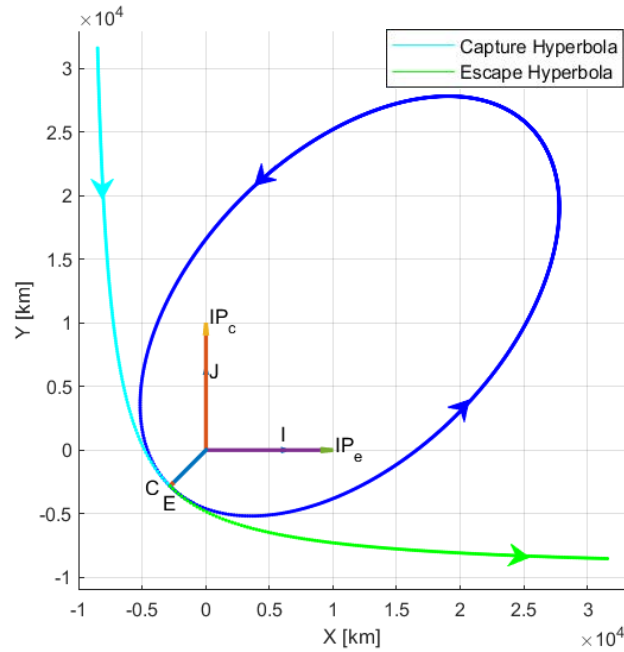


Figure 5.11: Problem geometry for $\alpha_c = 90^\circ - \alpha_e = 0^\circ$

2. $\alpha_c = 270^\circ - \alpha_e = 180^\circ$

This second case aims to study the behaviour of the genetic algorithm with a 315° rotation of the coplanar and symmetrical problem analyzed above. Optimized variables and output data for this study case are shown in Table 5.8 while the problem geometry is illustrated in Fig 5.12. The same global considerations did before for the study case 1 can be done here, where the orientation of the stopover orbit is symmetric to the bisector of the first and third quadrant.

Results	Value	UM
ΔV_{capt}	0.6941	km/s
ΔV_{esc}	0.6941	km/s
ΔV_{tot}	1.3882	km/s
ω	185.61	°
Ω	39.39	°
ρ_c	185.62	°
ρ_e	185.62	°
e_c	1.4142	/
e_e	1.4142	/
$\vec{V}_{orbit-c}$	[-3.104, 3.104, 0]	km/s
$\vec{V}_{orbit-e}$	[-3.104, 3.104, 0]	km/s
\vec{V}_{hyp-c}	[-3.595, 3.595, 0]	km/s
\vec{V}_{hyp-e}	[-3.595, 3.595, 0]	km/s
\vec{W}_{h-c}	[0, 0, 1]	/
\vec{W}_{h-e}	[0, 0, 1]	/

Table 5.8: Results for $\alpha_c = 270^\circ - \alpha_e = 180^\circ$

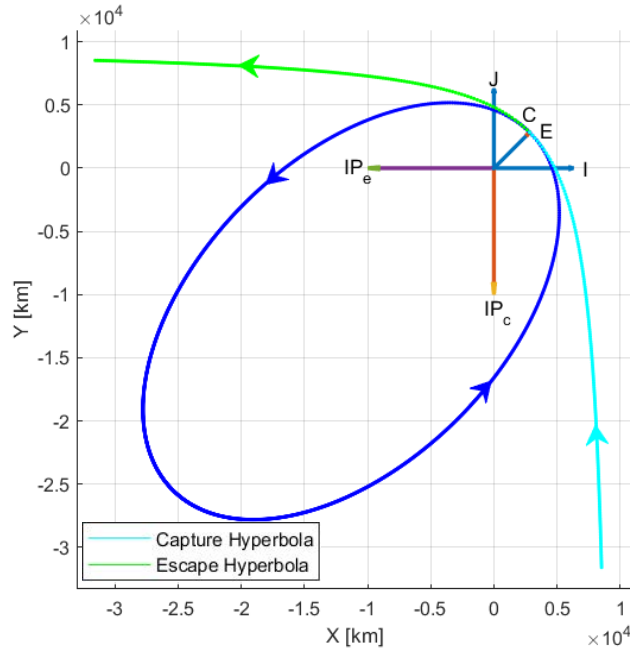


Figure 5.12: Problem geometry for $\alpha_c = 270^\circ - \alpha_e = 180^\circ$

5.3.2 Not identical rotation for capture and escape hyperbolic asymptotes

This section treats the coplanar problem from another point of view. The energy level is fixed, but the Right Ascension value is chosen to do not permit to have the capture and escape burns to the periapsis of the stopover orbit. Thus, the rotation for the capture and escape asymptotes is not the same. The chosen values for the Right Ascension are the following ones:

- $\alpha_c = 135^\circ$
- $\alpha_e = -45^\circ$

In this case, the entire problem does not evolve as in the previous one, then, the solution is not well-known. The genetic algorithm, taking as input data the ones shown in Table 5.9, permits to generate results summarized in Table 5.10 while the problem geometry is illustrated in Fig.5.13 and Fig.5.14.

Input Data	value	UM
a	20000	km
e	0.8	/
i	0	$^\circ$
α_c	135	$^\circ$
δ_c	0	$^\circ$
C_{3c}	4.435	km^2/s^2
α_e	-45	$^\circ$
δ_e	0	$^\circ$
C_{3e}	4.435	km^2/s^2

Table 5.9: Input data - $\alpha_c = 135^\circ$ - $\alpha_e = -45^\circ$

From Table 5.10, it can be observed that, as written before, capture and escape manoeuvres are not performed at the periapsis point obtaining a higher total velocity increment. Moreover, the capture manoeuvre is performed at a stopover orbit point different from the one relative to the escape manoeuvre. Thus, this permits to obtain different velocity increments relative to the single manoeuvres. The angular momentum of the hyperbolas permits to define the type of motion that, in this case, is a direct one and it the same as the stopover orbit. This fact confirms that the optimum injection manoeuvre occurs when the direction of the motion in the hyperbola is in the same as the motion in the stopover orbit.

Results	Value	UM
ΔV_{capt}	0.8642	km/s
ΔV_{esc}	1.1553	km/s
ΔV_{tot}	2.0195	km/s
ω	164.02	°
Ω	77.07	°
ρ_c	237.86	°
ρ_e	52.41	°
e_c	1.4901	/
e_e	1.7224	/
$\vec{V}_{orbit-c}$	[3.434 , 0.779 , 0]	km/s
$\vec{V}_{orbit-e}$	[-0.174 , -2.494 , 0]	km/s
\vec{V}_{hyp-c}	[4.187 , 1.205 , 0]	km/s
\vec{V}_{hyp-e}	[-0.732 , -3.506 , 0]	km/s
\vec{W}_{h-c}	[0 , 0 , 1]	/
\vec{W}_{h-e}	[0 , 0 , 1]	/

Table 5.10: Results - $\alpha_c = 135^\circ$ - $\alpha_e = -45^\circ$

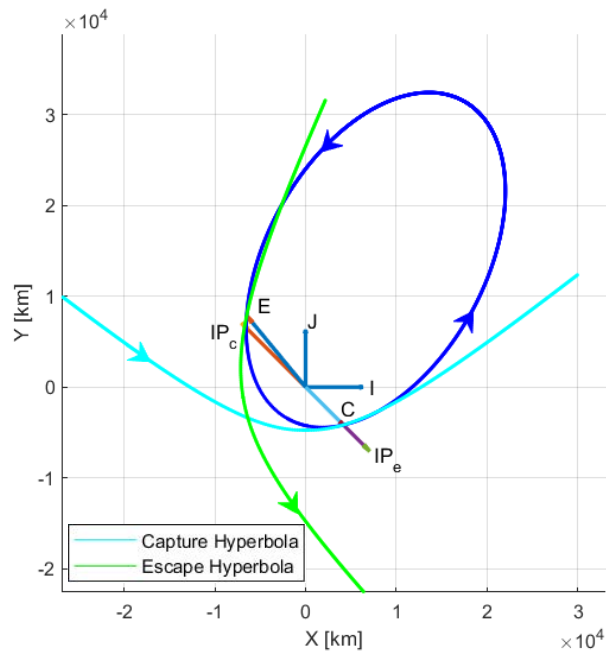


Figure 5.13: Problem geometry for $\alpha_c = 135^\circ$ - $\alpha_e = -45^\circ$

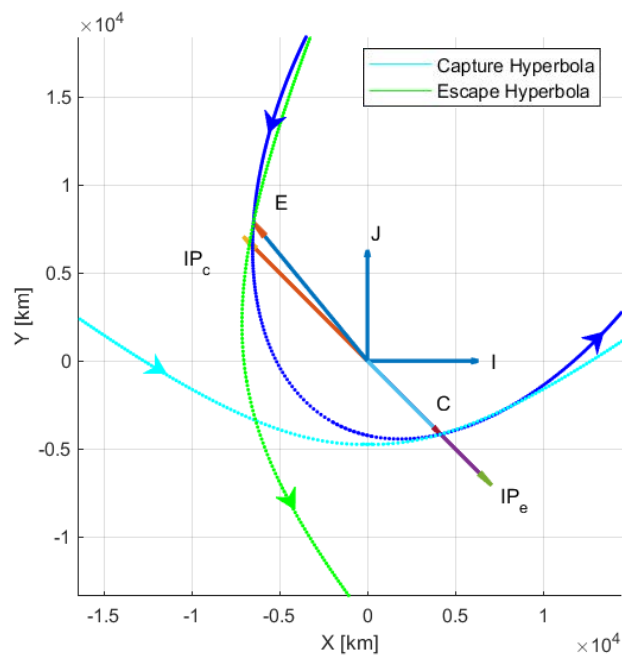


Figure 5.14: Problem geometry for $\alpha_c = 135^\circ - \alpha_e = -45^\circ$ - Zoom

5.4 Non-coplanar problem

This section aims to analyze a three-dimensional problem where non-coplanar conditions are assigned. This type of problem is more realistic than the coplanar one where the entire motion lies on the same plane. The optimum position for capture and escape manoeuvres not necessarily occurs at the periapsis of the stopover orbit so a ΔV penalty results due to the path angle and the plane change. The case here treated takes as input data those relative to a past Mars mission designed to be performed in 1974. They are shown in Table 5.11, where the right ascension and declination values are defined as the the direction of the hyperbolic excess velocity that coincides with the direction of the hyperbolic asymptotes. The genetic algorithm, taking these input data, has been generated the results reported in Table 5.12. Moreover, thanks to these, the problem geometry was plotted and is here reported in Fig.5.15 and Fig.5.16.

Input Data	value	UM
a	20000	km
e	0.8	/
i	170	$^\circ$
α_c	138	$^\circ$
δ_c	5.9	$^\circ$
C_{3c}	20.6	km^2/s^2
α_e	31.6	$^\circ$
δ_e	8.9	$^\circ$
C_{3e}	57.6	km^2/s^2

Table 5.11: Input data - Non-coplanar problem

Observing the results obtained from the optimization algorithm some considerations may be done. The capture and escape manoeuvres are performed on hyperbolas characterized by an inclination value similar to the stopover orbit one so, the entire motion is retrograde. In this case, both manoeuvres are performed when the general direction of the stopover orbit is the same as the direction of the hyperbolas minimizing the total velocity increment. Both manoeuvres are performed not so far from the periapsis point permitting to have a higher stopover orbit velocities reducing the total manoeuvre cost. Lastly, it can be observed as the velocity increment of the capture manoeuvre is less than the escape one due to the lower difference, in terms of magnitude and direction, from the velocities before and after the burn.

Results	Value	UM
ΔV_{capt}	2.785	<i>km/s</i>
ΔV_{esc}	4.768	<i>km/s</i>
ΔV_{tot}	7.553	<i>km/s</i>
ω	360	°
Ω	95.230	°
ρ_c	96.834	°
ρ_e	309.578	°
$\vec{V}_{orbit-c}$	[1.868 , -2.288 , 0.291]	<i>km/s</i>
$\vec{V}_{orbit-e}$	[3.303 , 2.211 , 0.616]	<i>km/s</i>
\vec{V}_{hyp-c}	[2.599 , -4.978 , 0.252]	<i>km/s</i>
\vec{V}_{hyp-e}	[6.433 , 5.756 , 1.209]	<i>km/s</i>
\hat{i}_{h-c}	169.73	°
\hat{i}_{h-e}	170.05	°
a_{h-c}	-2079	<i>km</i>
a_{h-e}	-743.541	<i>km</i>
e_c	4.165	/
e_e	7.050	/
ω_{h-c}	68.679	°
ω_{h-e}	325.446	°
Ω_{h-c}	103.223	°
Ω_{h-e}	94.8525	°
\hat{W}_{h-c}	[0.173 , 0.041 , -0.984]	/
\hat{W}_{h-e}	[0.172 , 0.0146 , -0.985]	/

Table 5.12: Results - Non-coplanar problem

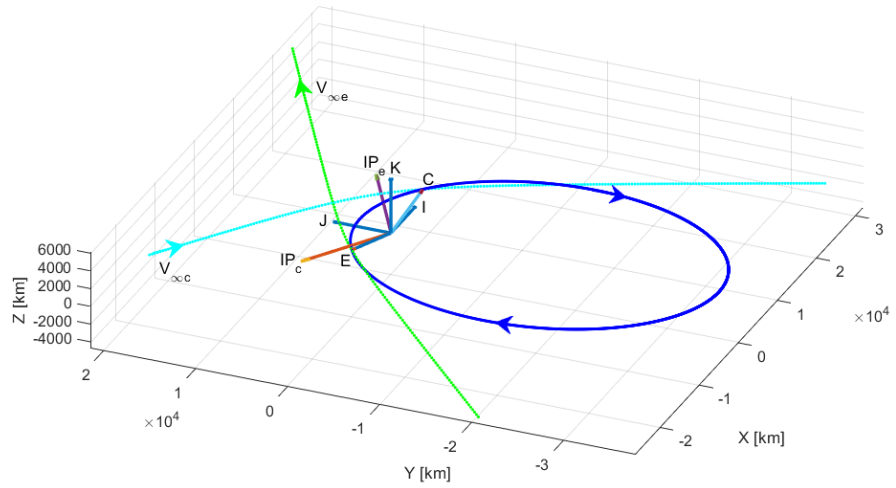


Figure 5.15: Non-coplanar problem geometry

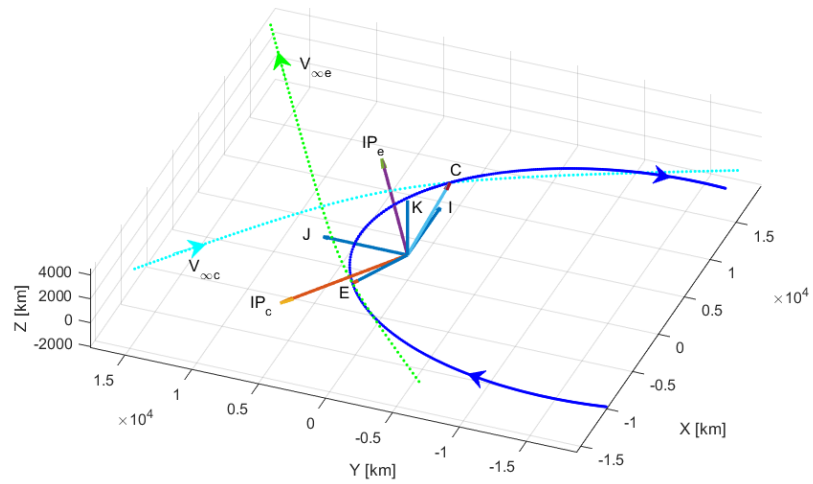


Figure 5.16: Non-coplanar problem geometry - Zoom

5.5 Variation of the periapsis distance

This section aims to study the total velocity increment varying the periapsis distance of the stopover orbit within the range $[50–1000] km$ (defined as the altitude from the Mars surface). The periapsis distance is a function of two parameters:

- Semimajor-axis a
- Eccentricity e

For the case here treated, the semimajor axis is assumed constant while the eccentricity varies according to the following equation:

$$e = 1 - \frac{r_p}{a} \quad (5.7)$$

This study case is based on the input data reported in Table 5.13 and, by means of the optimization algorithm, is characterized by the results shown in Table 5.14. Moreover, the trend of total velocity increment respect to the periapsis distance is illustrated in Fig. 5.18.

Input Data	value	UM
a	19550	km
i	170	$^\circ$
α_c	138	$^\circ$
δ_c	5.9	$^\circ$
C_{3c}	20.6	km^2/s^2
α_e	31.6	$^\circ$
δ_e	8.9	$^\circ$
C_{3e}	57.6	km^2/s^2

Table 5.13: Input data - Variation of the periapsis distance

Observing Table 5.14 and Fig. 5.18 it can be noted that a periapsis distance increase causes a total velocity increment raise. It is increased by 5% within the chosen range. Analyzing the capture and escape velocity increment, it can be observed as the capture ΔV is higher than the escape one. Moreover, observing Fig.5.17 it can be noted that the capture velocity increment does not vary with the periapsis distance and then remains constant while, the escape velocity increment increases by 10%. At the same time, the orientation of the stopover orbit changes. The Right Ascension of the Ascending Node remains almost constant while the Argument of periapsis moves, increasing the distance from the Line of the Ascending Node. Due to the variation of the stopover orbit orientation, the capture and escape manoeuvres are performed at different points. For the

capture manoeuvres, it can be observed as it is performed at points getting closer to the periapsis while for the escape burn, the behaviour is different. Here, the manoeuvre is accomplished at the same point of the stopover orbit, characterized by the same true anomaly ($\rho - \omega$).

$h[km]$	$\Delta V[km/s]$	$\Delta V_c[km/s]$	$\Delta V_e[km/s]$	$\omega[^\circ]$	$\Omega[^\circ]$	$\rho_c[^\circ]$	$\rho_e[^\circ]$
50	7.441	2.805	4.636	70.948	167.951	174.178	18.729
100	7.457	2.802	4.655	70.911	167.698	173.464	18.708
150	7.474	2.801	4.673	70.500	167.069	172.468	18.327
200	7.488	2.800	4.688	71.681	167.688	172.835	19.167
250	7.504	2.799	4.705	71.905	167.910	172.353	19.569
300	7.520	2.798	4.722	70.668	166.490	170.685	18.487
350	7.535	2.784	4.751	72.333	167.730	171.414	19.772
400	7.550	2.791	4.759	72.196	167.667	171.014	20.240
450	7.565	2.796	4.769	73.463	168.481	171.460	21.032
500	7.580	2.795	4.785	73.365	167.919	170.662	20.692
550	7.595	2.794	4.801	73.059	167.601	169.920	20.643
600	7.610	2.784	4.826	73.596	167.852	169.774	21.015
650	7.625	2.786	4.839	71.894	166.131	167.597	19.551
700	7.638	2.795	4.843	74.834	168.683	169.969	22.174
750	7.653	2.794	4.859	75.175	168.987	169.702	22.832
800	7.667	2.797	4.870	74.947	168.531	168.868	22.465
850	7.681	2.792	4.889	75.189	168.624	168.495	22.698
900	7.696	2.795	4.901	76.288	169.151	168.888	23.523
950	7.710	2.793	4.917	76.193	168.899	168.411	23.428
1000	7.723	2.796	4.927	75.927	168.397	167.535	22.760

Table 5.14: Results - Variation of the periapsis distance

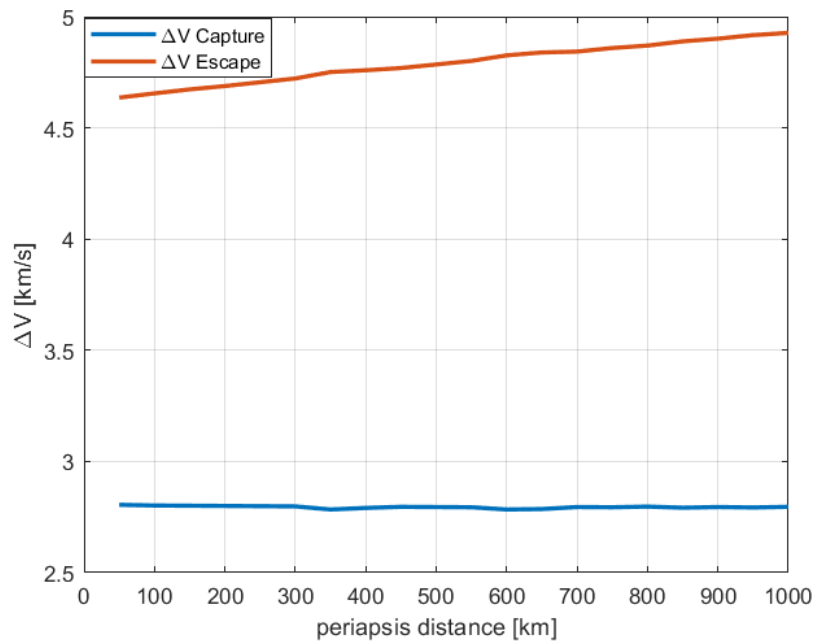


Figure 5.17: ΔV for capture and escape manoeuvres - Periapsis Distance

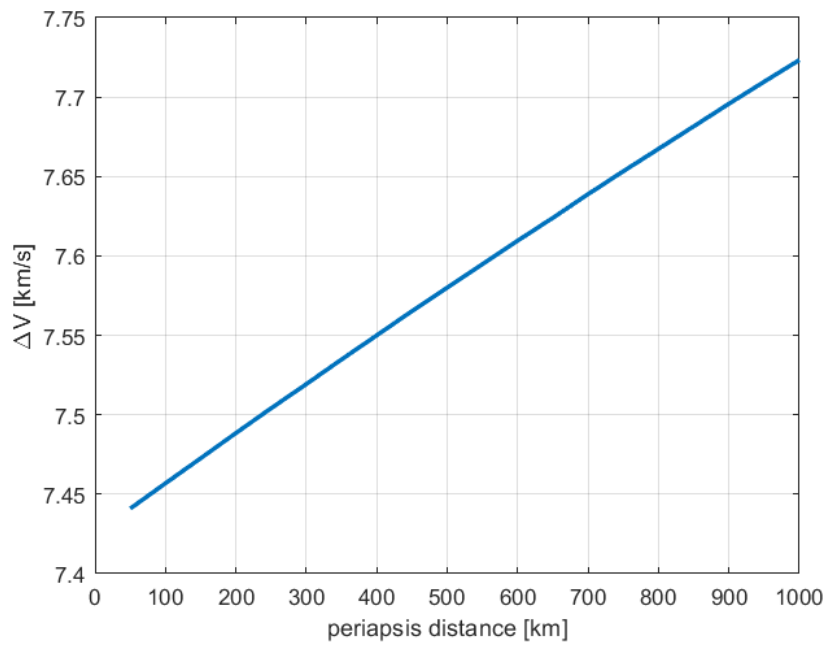


Figure 5.18: ΔV - Periapsis Distance

5.6 Variation of the semimajor axis

This section concerns the study of the total velocity increment when the semimajor axis of the stopover orbit varies. As written before, there is a relationship between the semimajor axis, the eccentricity and the periapsis distance of a certain orbit. This one is given by the following equation:

$$a = \frac{r_p}{1 - e} \quad (5.8)$$

Thus, there are two methods to obtain a semimajor axis variation:

- variation of the eccentricity fixing the periapsis distance
- variation of the periapsis distance fixing the eccentricity

In this case, the first method is used to permit to the semimajor axis to vary between $10000km$ and $30000km$. Input data are shown in Table 5.15 while results are presented in Table 5.16. Moreover, the variation of the total velocity increment respect to the semimajor axis value is illustrated in Fig.5.20.

Input Data	value	UM
r_p	500	km
i	170	°
α_c	138	°
δ_c	5.9	°
C_{3c}	20.6	km ² /s ²
α_e	31.6	°
δ_e	8.9	°
C_{3e}	57.6	km ² /s ²

Table 5.15: Input data - Variation of the semimajor axis of the stopover orbit

From Table 5.15 or from Fig.5.20 it can be observed as the total velocity increment decreases if the semimajor axis of the stopover orbit raises. This variation, of about 5%, is due to the decrement of the ΔV needed for the escape manoeuvre while the capture velocity increment remains almost constant. This behaviour can be observed in Fig5.20, where the velocity increment for both manoeuvres compared with the semimajor axis of the stopover orbit is plotted. Moreover, it can be noted as the cost of the escape manoeuvre is higher than the capture one. Fixing the starting conditions and varying the stopover orbit semimajor axis the orientation of this orbit does not change much. The Line of the Ascending Node, which position is described by Ω , varies its angular position of about 2° in the worst case while the Argument of Periapsis ω and then the

periapsis position varies, in the worst case, of about 5° respect to the Line of the Ascending node.

$a[km]$	$\Delta V[km/s]$	$\Delta V_c[km/s]$	$\Delta V_e[km/s]$	$\omega[^\circ]$	$\Omega[^\circ]$	$\rho_c[^\circ]$	$\rho_e[^\circ]$
10000	7.840	2.855	4.985	74.212	166.500	162.274	22.480
11000	7.791	2.839	4.952	75.906	168.458	165.583	23.809
12000	7.750	2.822	4.928	75.834	168.943	167.006	23.748
13000	7.716	2.819	4.897	75.544	168.882	167.922	23.416
14000	7.687	2.816	4.871	73.608	167.325	167.017	21.416
15000	7.662	2.810	4.852	74.809	168.585	168.946	22.316
16000	7.640	2.807	4.833	74.609	168.791	169.893	22.273
17000	7.620	2.801	4.820	74.400	168.452	170.013	21.780
18000	7.603	2.783	4.821	71.998	166.587	168.588	19.662
19000	7.588	2.796	4.793	73.666	168.353	170.745	21.244
20000	7.574	2.780	4.795	74.432	169.291	172.245	21.928
21000	7.562	2.789	4.773	73.323	168.139	171.276	20.867
22000	7.550	2.788	4.762	73.750	168.853	172.201	21.182
23000	7.534	2.785	4.754	72.400	167.673	171.414	20.002
24000	7.530	2.783	4.747	70.708	166.165	170.066	18.418
25000	7.522	2.787	4.735	72.796	168.139	172.259	20.226
26000	7.513	2.790	4.724	72.322	167.930	172.340	20.031
27000	7.506	2.778	4.728	70.800	166.477	171.027	18.487
28000	7.499	2.780	4.719	72.142	167.965	172.741	19.860
29000	7.492	2.771	4.721	71.990	167.767	172.752	19.631
30000	7.487	2.780	4.707	72.900	168.857	173.964	20.737

Table 5.16: Results - Variation of the semimajor axis of the stopover orbit

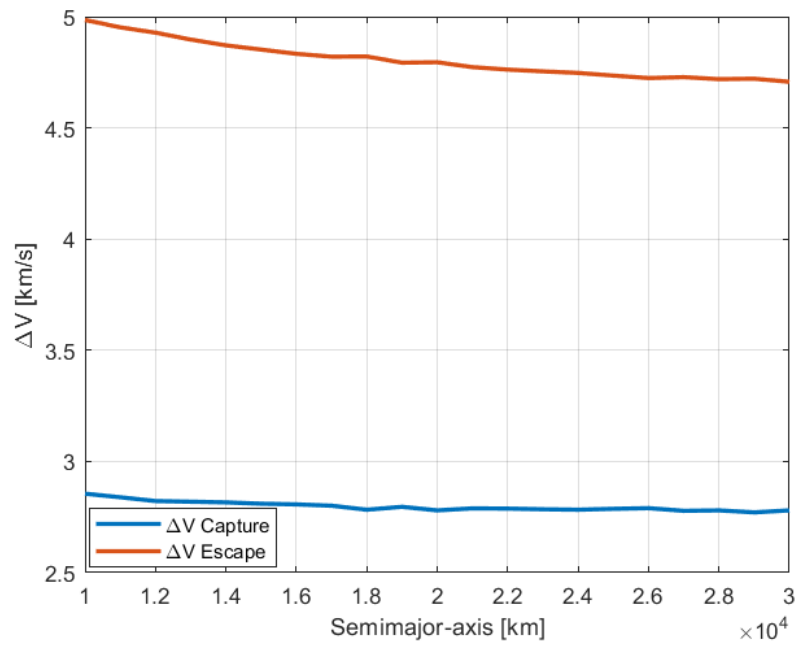


Figure 5.19: ΔV for capture and escape manoeuvres - Semimajor-axis

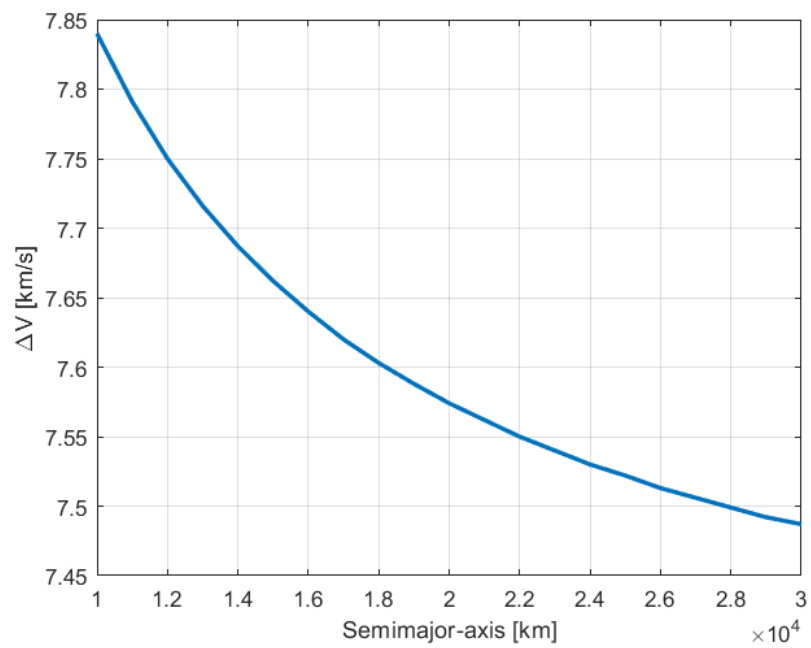


Figure 5.20: ΔV - Semimajor axis

5.7 Complete problem: implementation of the Descent - Ascent Manoeuvres

This section aims to study and define the best parking orbit geometry for a case in which capture, escape, descent and ascent manoeuvres are taken into account. These four phases are the most important ones performed within the Mars Sphere of Influence and affect the total propellant consumption. The section is divided into two parts. The first one is relative to the problem where the orbit geometry changes in terms of periapsis distance for a fixed semimajor axis while the second one is referred to the opposite case. Thus, in the second study case, the total velocity increment will be evaluated as a function of the variation of the semimajor axis for a fixed periapsis distance.

5.7.1 Variation of the periapsis distance

This study case exploits the input data reported in Table 5.17. The descent and ascent manoeuvres are now taking into account, and their contributions to the total velocity increment are now evaluated. The results obtained for a periapsis distance variation, within the range [50 – 1000km] from the Mars surface, are reported in Table while Fig.5.21 and Fig.5.22 show, respectively, the contributions of the descent and ascent manoeuvres and the total velocity increment. It can be noted that the contribution of the descent manoeuvre is really small respect to the others and does not change much within the periapsis range. On the opposite side, the ascent manoeuvre has a great impact on the total propellant consumption. It decreases if the periapsis distance raises and then, in terms of cost, it is cheaper to perform this manoeuvre at a higher distance from the Mars surface. The decrease of the propellant consumption of the ascent manoeuvre is more rapid than the increase of the ΔV to perform capture and escape phases, then, the total velocity increment decrease. This trend can be observed in Fig.5.22, where the total ΔV is reported as a function of the periapsis distance. Thus, the choice of the stopover for this study case is principally affected by the ascent manoeuvre that defines the best stopover orbit like the one characterized by with the higher periapsis distance.

$h[km]$	$\Delta V_{orbit}[km/s]$	$\Delta V_{descent}[km/s]$	$\Delta V_{ascem}[km/s]$	$\Delta V_{TOT}[km/s]$
50	7.441	1.250	5.048	13.739
100	7.457	1.250	5.010	13.718
150	7.474	1.251	4.974	13.697
200	7.488	1.251	4.938	13.677
250	7.504	1.251	4.902	13.657
300	7.520	1.251	4.868	13.638
350	7.535	1.251	4.834	13.620
400	7.550	1.251	4.800	13.601
450	7.565	1.251	4.768	13.584
500	7.580	1.251	4.736	13.566
550	7.595	1.251	4.704	13.550
600	7.610	1.250	4.673	13.533
650	7.625	1.250	4.643	13.517
700	7.638	1.250	4.613	13.501
750	7.653	1.249	4.584	13.486
800	7.667	1.249	4.555	13.471
850	7.681	1.248	4.527	13.456
900	7.696	1.247	4.499	13.442
950	7.710	1.247	4.471	13.428
1000	7.723	1.246	4.444	13.414

Table 5.17: Results - Variation of the periapsis distance of the stopover orbit for capture, escape, descent and ascent manoeuvres

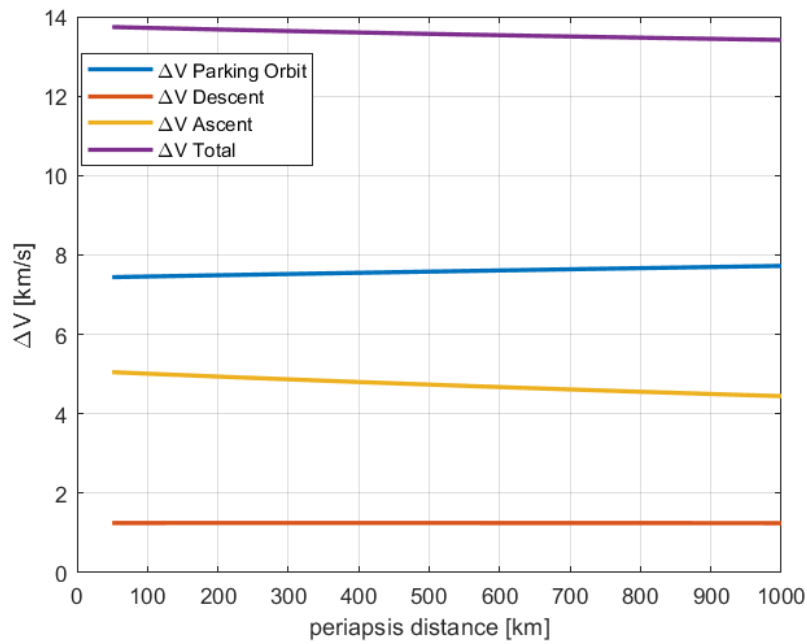


Figure 5.21: ΔV - Periapsis Distance for capture, escape, descent and ascent manoeuvres

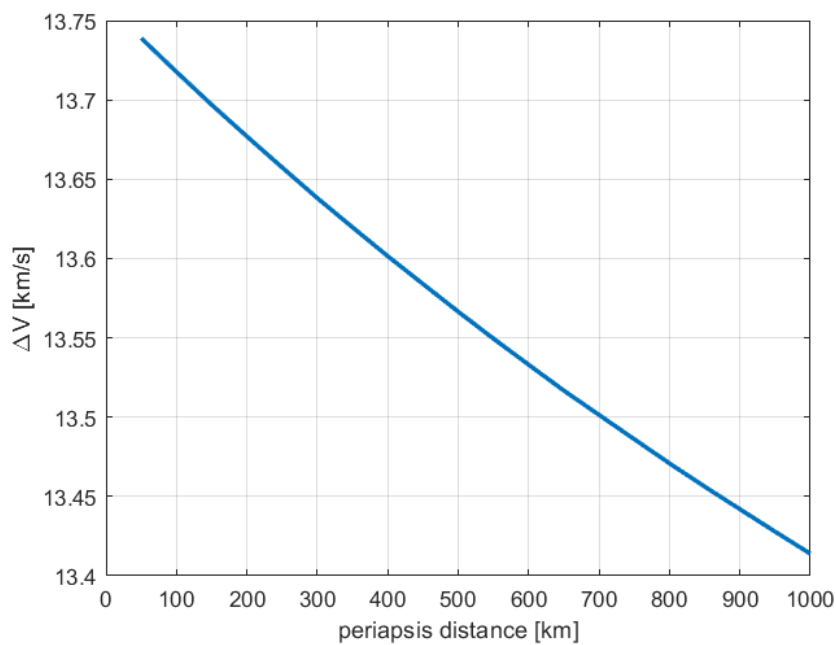


Figure 5.22: ΔV_{TOT} - Periapsis Distance for capture, escape, descent and ascent manoeuvres

5.7.2 Variation of the semimajor axis

This second study case concerns the study of the complete problem (capture, escape, ascent and descent manoeuvres are considered) when the semimajor axis of the stopover orbit varies within the range [10000 : 30000]km with a fixed periapsis distance (500km) from the Mars surface. The input data are relative to the previous case, where only capture and escape manoeuvres were considered (Table 5.13), while results are summarised in Table 5.18. Results show that the trend of the velocity increment for ascent and descent manoeuvres are different. The descent manoeuvre, which permits to land on the Martian surface, varies with a positive trend of about 30% increasing then the total cost. This increase is due to the higher periapsis velocity of the stopover orbit, in fact, if the energy equation is taken into account, it can be noted that for a fixed periapsis distance an increment of the semimajor axis causes a velocity increase at that point. Thus, for the same transfer orbit, the breaking manoeuvre that permits to land on the Martian surface has to be greater. The same consideration may be done for the ascent manoeuvre where the Mars Ascent Vehicle will leave the Martian surface to reach the desired stopover orbit. The increase of the semimajor axis of the parking orbit imposes a higher periapsis velocity so, for the same transfer orbit and the same starting conditions the manoeuvre that it needs is characterized by a higher ΔV . Lastly, from Fig.5.24 it can be observed as the increment of the ΔV for the descent and ascent manoeuvres implies an increase of the total propellant consumption even if the velocity increment for the capture/escape phases decreases. Thus, the desirable stopover orbit for the case in which the periapsis distance is fixed has to be characterized by a small semimajor axis value.

$a[km]$	$\Delta V_{orbit}[km/s]$	$\Delta V_{descent}[km/s]$	$\Delta V_{ascent}[km/s]$	$\Delta V_{TOT}[km/s]$
10000	7.840	1.009	4.494	13.343
11000	7.791	1.055	4.540	13.386
12000	7.750	1.093	4.578	13.421
13000	7.716	1.125	4.610	13.451
14000	7.687	1.152	4.637	13.476
15000	7.662	1.176	4.660	13.498
16000	7.640	1.196	4.681	13.517
17000	7.620	1.214	4.699	13.532
18000	7.603	1.230	4.714	13.547
19000	7.588	1.244	4.728	13.560
20000	7.574	1.256	4.741	13.571
21000	7.562	1.268	4.753	13.582
22000	7.550	1.278	4.763	13.591
23000	7.534	1.288	4.772	13.600
24000	7.530	1.296	4.781	13.607
25000	7.522	1.304	4.789	13.615
26000	7.513	1.311	4.796	13.621
27000	7.506	1.318	4.803	13.627
28000	7.499	1.324	4.809	13.633
29000	7.492	1.330	4.815	13.637
30000	7.487	1.336	4.820	13.643

Table 5.18: Output data - Variation of the semimajor axis of the stopover orbit for capture, escape, descent and ascent manoeuvres

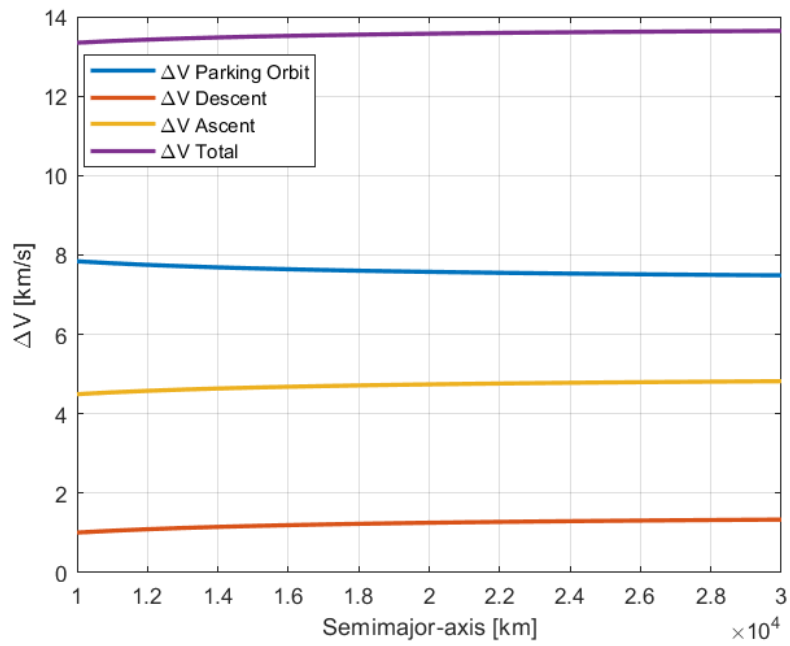


Figure 5.23: ΔV - Semimajor axis for capture, escape, descent and ascent manoeuvres

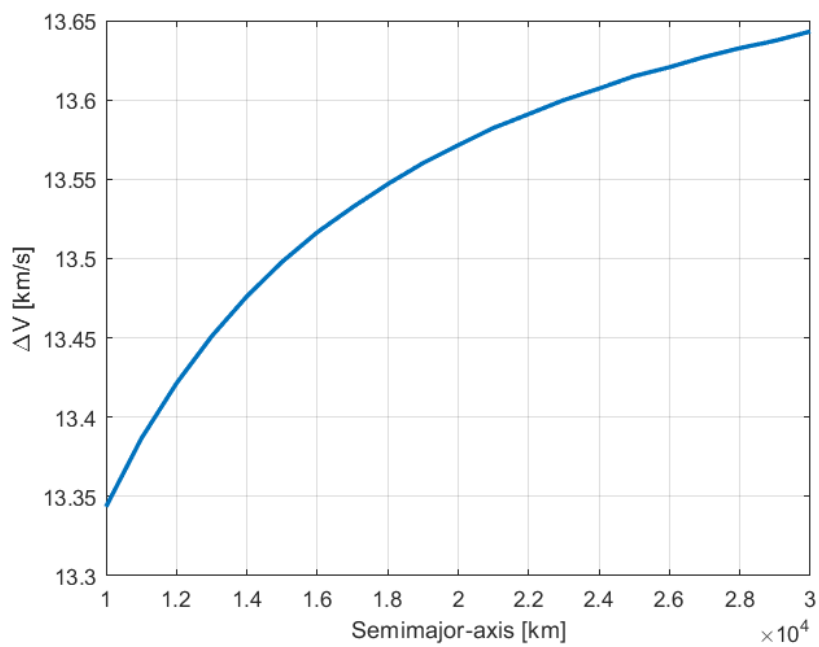


Figure 5.24: ΔV_{TOT} - Semimajor axis for capture, escape, descent and ascent manoeuvres

Chapter 6

Conclusions & Future Works

The purpose of this Master Thesis was relating to the development, implementation, and successive exploitation of an algorithm able to evaluate the parking orbit orientation and the manoeuvres positions for a capture and escape mission minimizing the total velocity increment.

This algorithm was implemented on the idea to generate a support tool for the trajectory design relative to a future Mars Sample Return Mission that, is one of the primary goals for the next decade into the field of space exploration. This tool may be useful to study and evaluate the different mission phases relative to the parking orbit definition, such as the descent on the Mars surface and the ascent to the stopover orbit, and also for understanding the behaviour of this orbit inside the planet's perturbations environment. Aiming to go into the details of the problem, the Mars Sample Return mission led by ESA and NASA was, first of all, introduced so that they can understand the different phases that will characterize the entire mission. After that, the focus was moved on the type of algorithms exploited to solve the optimization problem and so, an introduction of what they are and what they do the genetic algorithms has been done. These algorithms due to their higher computational capacity are efficient solver method to study multi-variables problems into a wide solution search space and then, they were chosen for the purpose to solve the parking orbit definition problem. The optimization algorithm was introduced going to describe the physical methods exploited to simplify the problem and then, the calculation procedure was explained. The algorithm presented was implemented by MATLAB and for the purpose to validate it, some tests were executed. First of all, a coplanar and symmetrical problem evolving on the Mars equatorial plane (zero inclination and zero declination) was considered because the analytical solution was well-known. The same problem was studied with reverse starting conditions to evaluate the algorithm behaviour with retrograde conditions. In both cases, the computational results are the same as the analytical ones and then, the algorithm was validated. Subsequently, the coplanar and

symmetrical problem was tested varying the Right Ascension and the stopover orbit inclination obtaining, as it was intended to be, the same results of the previous cases. The last validation test was performed for a three-dimensional study case, where capture and escape manoeuvres were not performed on the same plane, obtaining congruent results relative to the logic problem. In fact, Table 5.12 and Fig.5.15 show that the optimum injection manoeuvres were performed in the proximity of the stopover orbit periapsis on hyperbolic trajectories characterized by the inclination value similar to the stopover orbit one. Moreover, this study case helped the analysis relative to the orbit geometry variation where two different cases were considered. The first one was relative to the periapsis distance variation for a fixed semimajor axis value while the second one was referred to a case in which the semimajor axis varied for a fixed periapsis distance. In the first case, the increase of the periapsis distance causes an increment of the propellant consumption while in the opposite case the total cost of the manoeuvres decreases. Thus, for a fixed semimajor axis the best stopover orbit is the one with the periapsis closer to the Martian surface. In the second case, where the periapsis distance was fixed to $500km$ from the Martian surface (possible parking orbit for the Mars Sample Return mission), the results show that incrementing the semimajor axis of the stopover orbit the total propellant consumption decreases. Thus, a stopover orbit with a high semimajor axis is desirable. Lastly, the problem of the orbit geometry variation was associated with the descent and ascent manoeuvres modeled by Hohmann transfer equations. Evaluating the contributions for both manoeuvres to the total velocity increment, the first two study cases of the orbit geometry variation was studied. In the first case, for a fixed semimajor axis, results show that the higher contribution is given by the capture and escape manoeuvres but the decrement of the ascent manoeuvres propellant consumption causes the decrease of the total velocity increment. In the second case, for a fixed periapsis distance, the behaviour of the total velocity increment is the opposite one. In fact, the propellant consumption relative to the ascent manoeuvre increases more than the decrement of the parking orbit ΔV and then the total velocity increment increase. In this case, when the semimajor axis value is equal to $10000km$ the minimum total velocity increment is calculated. This value is equal to $13.343km/s$. Lastly, in both cases, the propellant consumption relative to the descent manoeuvres, remaining almost constant, was the minimum one.

Thanks to these final studies, where all manoeuvres were taken into account, the results show the importance of the ascent and descent manoeuvres that so, have to be considered for the parking orbit definition. The work here discussed is based on the idea to provide support for the future Mars Sample Return mission programmed to start in 2020. The optimization algorithm is able to treat the perturbative problem where perturbations due to planet's oblateness are not neglected

but, due to lack of time, it has not been treated. In this case, the code has to be modified and equations relative to planet's oblateness perturbations have to be inserted inside the code. This future implementation will permit to analyze the three-dimensional problem not only as a function of the stopover orbit geometry but also as a function of the stopover time that can affect in a positive or negative way the total propellant consumption. Moreover, other mission requirements and constraints, such as communication ones, may be taken into account and then, the parking orbit geometry may be change. In fact, to have a synchronous orbit and then, to optimize the communications operations between the orbiter and the systems on the Mars surface, a parking orbit with a semimajor axis of about $20000km$ must be selected. Then, knowing the total velocity increment, the masses calculation, relative to the different systems, can be executed and optimized for different propulsive architectures. The ascent phase may be implemented utilizing a more accurate method where losses will be estimated in detail, and then, the staging process may be executed to optimize the Mars Ascent Vehicle design. Lastly, the efficiency of the optimization algorithm may be improved by compacting the code and by studying the best optimization options for the genetic algorithm solver.

Bibliography

- [1] S.Squyres, "*Vision and Voyages for Planetary Science in the Decade 2013–2022. Committee on the Planetary Science Decadal Survey; National Research Council*", 2011.
- [2] International MSR Objectives and Samples Team (iMOST), "*The Potential Science and Engineering Value of Samples Delivered to Earth by Mars Sample Return*", August 14, 2018.
- [3] M. Schulte, M. Meyer, J. Grant and M. Golombek, "*The Mars 2020 Rover Mission Landing Site Candidates*", *2nd International Mars Sample Return 2018*, 2018.
- [4] S. Centuori, P. Hermosín, J. Martín, G. De Zaiacomo, S. Colin, A. Godfrey, J. Myles, H. Johnson, T. Sachdev, R. Ahmed, "*Mars Sample Return Architecture Assessment Study*", *2nd International Mars Sample Return 2018*, 2018.
- [5] C.R. Neal, C.K. Shearer, M.Wadwha L. Borg,B. Jolliff, A. Treiman, "*Developing Sample Return Technology using the Earth's Moon as a Testing Ground*",
- [6] C. D. Edwards and S. Vijendran, "*Mars Sample Return Architecture Overview*", *2nd International Mars Sample Return 2018*, 2018.
- [7] National Aeronautics and Space Administration, "*Mission Concept Study: Planetary Science Decadal Survey—MSR Lander Mission*", Science Champion: Phil Christensen , NASA HQ POC: Lisa May, April 2010.
- [8] iMars Working Group, "*Preliminary Planning for an International Mars Sample Return Mission* ", June 2008, available at <https://mepag.jpl.nasa.gov/reports>
- [9] R. Mattingly and L. May, "*Mars sample return as a campaign*", *Proc. IEEE Aerosp. Conf.*, Big Sky, MT, Mar. 2011, pp. 1–13
- [10] L. Duvet, F. Beyer, J. Delfa, E. Zekri, "*ESA Sample Fetch Rover: heritage and way forward*",*2nd International Mars Sample Return 2018*, 2018.

- [11] S. Vijendram, C.D. Edwards, B.K. Muirhead, J. Huesing, L. Duvet, F. Beyer, " *Mars Sample Return Engineering - A reference architecture for joint ESA-NASA studied and early mission concepts* " ,*EPSC Abstracts*, Vol.12, EPSX2018-1057-1, 2018.
- [12] U. Derz, E. Joffre, M-C. Perkinson, J. Huesing, F. Beyer, J.M. Sanchez Perez, Airbus Defence and Space Ltd, European Space Agency, " *Mars Sample Return Orbiter Architecture Options - Results of the ESA Mars Sample Return Architecture assessment study* " , *2nd International Mars Sample Return 2018*, 2018.
- [13] S. Vijendram, J. Huesing, F. Beyer, A. McSweeney " *Mars Sample Return - Earth Return Orbiter Mission Overview* " ,*2nd International Mars Sample Return 2018*, 2018.
- [14] H. Price, K. Cramer, S. Doudrick, W. Lee, J. Matijevic, S. Weinstein, T. Lam-Trong, O. Marsal, and R. Mitcheltree, " *Mars Sample Return Spacecraft Systems Architecture* " , *IEEE Aerospace Conference Proceedings*, 2000 pp. 357-375.
- [15] B. Panicucci, M. Pappalardo, M. Passacanto " *Introduzione all'optimisation toolbox di Matlab* " .
- [16] S. Sivanandam, S. Deepa, " *Genetic Algorithm implementation using MATLAB* " , in: *Introduction to genetic algorithm*, Springer, Berlin, Heidelberg, 2008, pp. 211-262.
- [17] P.A. Diaz-Gomez, D.F. Hougen, " *Initial Population for Genetic Algorithms: a Metric Approach* " , in: *in Proceedings of the 2007 International Conference on Genetic and Evolutionary Methods*, Las Vegas, Nevada, USA, 2007, pp. 43-49.
- [18] Allan H. Treiman, " *Groundbreaking Sample Return from Mars: The Next Giant Leap in Understanding the Red Planet* " ,Lunar and Planetary Institute, 3600 Bay Area Blvd., Houston TX 77058
- [19] P. Desai, R. Braun and R. Powell, " *Aspects of Parking Orbit Selection in a Manned Mars Mission* " NASA TP-3256, December 1992
- [20] D.E. Cornick and L.K. Seversike, " *Optimum Parking Orbit Orientation for a Three-Dimensional Capture-Escape Mission* " . *Journal of Spacecraft and Rockets*, Vol. 7, No. 7, 1970, pp. 808–813
- [21] P. Desai, J.J. Buglia, " *Determining Mars Parking Orbits that Ensure Tangential Periapsis Burns at Arrival and Departure* " . *Journal of Spacecraft and Rockets*, Vol. 30, No. 7, July-August 1993, pp.414-419

- [22] D.F. Landau, J.M. Longuski, P.A. Penzo “*Method for Parking Orbit Reorientation for Human Missions to Mars*”. Journal of Spacecraft and Rockets, Vol. 42, No. 3, May-june 2005, pp.517-522
- [23] R. W. Luidens, B. A. Miller, “*Efficient Planetary Parking Orbits With Examples For Mars*”. NASA TN D-3220
- [24] H. W. Small, “*Globally Optimal Parking Orbit Transfer*”. AIAA-82-1478, San Diego, California, August 9-11,1982.
- [25] A.B. Segeyevsky, G.C. Snyder, R.A. Cuniff, “*Interplanetary Mission Design Handbook, Volume 1, Part 2. Earth to Mars Ballistic Mission Opportunities, 1990-2005*”, JPL Publication 82-43, September 1983.
- [26] L.E. George, L.D. Kos, “*Interplanetary Mission Design Handbook: Earth to Mars Mission Opportunities and Mars to Earth Return opportunities, 2009-2024*”, NASA/TM-1998-208503, July 1998.
- [27] L.M. Burke, R.D. Falck, M.L. McGuire, “*Interplanetary Mission Design Handbook: Earth to Mars Mission Opportunities 2026 to 2045*”, NASA/TM-2010-216764, October 2010.
- [28] G. Avanzini, G. Colasurdo, “*Astrodynamics*”, Politecnico di Torino, 2006.
- [29] L.M. Burke, D.F. Falck, M.L. McGuire, *Fundamentals of Astrodynamics* Dover Publications Inc, New York, 1971.
- [30] Mars Sample Return - Jet Propulsion Laboratory, <https://www.jpl.nasa.gov/missions/mars-sample-return-msr/>.
- [31] Mars Sample Return - European Space Agency, <https://www.jpl.nasa.gov/missions/mars-sample-return-msr/>.
- [32] NASA - Mars Exploration Program, <https://mars.nasa.gov/>.
- [33] ESA - Mars Sample Return, <http://exploration.esa.int/mars/44995-mars-sample-return/>.
- [34] MATHWORKS - ga solver, <https://www.mathworks.com/help/gads/ga.html>.